NASA TECHNICAL NOTE

NASA TN D-7852

NASA TN D-7852

PARAMETRIC STUDIES WITH AN ATMOSPHERIC DIFFUSION MODEL THAT ASSESSES TOXIC FUEL HAZARDS DUE TO THE GROUND CLOUDS GENERATED BY ROCKET LAUNCHES

Roger B. Stewart and William L. Grose

Langley Research Center

Hampton, Va. 23665

NATIONAL AERONAUTICS AND SPACE ADMINISTRATION • WASHINGTON, D. C. • MAY 1975

1. Report No.	2. Government Accession No.	3. Recipient's Catalog No.
NASA TN D-7852		

4. Title and Subtitle	5. Report Date
PARAMETRIC STUDIES WITH AN ATMOSPHERIC DIFFUSION MODEL THAT ASSESSES TOXIC FUEL HAZARDS DUE TO THE GROUND CLOUDS GENERATED BY ROCKET LAUNCHES	May 1975
	6. Performing Organization Code

7. Author(s)	8. Performing Organization Report No.
Roger B. Stewart and William L. Grose	L-9694
	10. Work Unit No.
	180-72-50-01

9. Performing Organization Name and Address	11. Contract or Grant No.
NASA Langley Research Center Hampton, Va. 23665	
	13. Type of Report and Period Covered
	Technical Note

12. Sponsoring Agency Name and Address	14. Sponsoring Agency Code
National Aeronautics and Space Administration Washington, D.C. 20546	

15. Supplementary Notes

16. Abstract

Parametric studies were made with a multilayer atmospheric diffusion model to place quantitative limits on the uncertainty of predicting ground-level toxic rocket-fuel concentrations. The features of greatest interest involve the exhaust distributions in the ground cloud, cloud stabilized geometry, atmospheric diffusion coefficients, the effects of exhaust plume afterburning of carbon monoxide CO, assumed surface mixing-layer division in the model, and model sensitivity to different meteorological regimes. Depending on assumed input parameters, large-scale differences in ground-level predictions were quantitatively described. The model characterization of cloud alongwind growth for several meteorological conditions was shown to be in error because of incorrect application of previous diffusion theory. In addition, rocket-plume calculations indicate that almost all of the rocket-motor carbon monoxide is afterburned to carbon dioxide CO_2, thus reducing toxic hazards due to CO. The afterburning was also shown to have a significant effect on cloud stabilization height and on ground-level concentrations of exhaust products.

17. Key Words (Suggested by Author(s))	18. Distribution Statement
Atmospheric diffusion Toxic rocket-fuel hazards	Unclassified – Unlimited New Subject Category 46

19. Security Classif. (of this report)	20. Security Classif. (of this page)	21. No. of Pages	22. Price*
Unclassified	Unclassified	63	$4.25

*For sale by the National Technical Information Service, Springfield, Virginia 22151

PARAMETRIC STUDIES WITH AN ATMOSPHERIC DIFFUSION MODEL THAT ASSESSES TOXIC FUEL HAZARDS DUE TO THE GROUND CLOUDS GENERATED BY ROCKET LAUNCHES

Roger B. Stewart and William L. Grose
Langley Research Center

SUMMARY

Parametric studies were made with a multilayer atmospheric diffusion model to place quantitative limits on the uncertainty of predicting ground-level toxic rocket-fuel concentrations. The features of greatest interest involve the exhaust distributions in the ground cloud, cloud stabilized geometry, atmospheric diffusion coefficients, the effects of exhaust plume afterburning of carbon monoxide CO, assumed surface mixing-layer division in the model, and model sensitivity to different meteorological regimes. Depending on assumed input parameters, large-scale differences in ground-level predictions were quantitatively described. The model characterization of cloud alongwind growth for several meteorological conditions was shown to be in error because of incorrect application of previous diffusion theory. In addition, rocket-plume calculations indicate that almost all of the rocket-motor carbon monoxide is afterburned to carbon dioxide CO_2, thus reducing toxic hazards due to CO. The afterburning was also shown to have a significant effect on cloud stabilization height and on ground-level concentrations of exhaust products.

INTRODUCTION

Rockets release large quantities of hot, buoyant exhaust products into the atmosphere during launch. In sufficient concentration, some of the products are toxic and pose potential hazards to health and the environment (ref. 1). The National Environmental Policy Act of 1969 makes an environmental impact statement mandatory for any Federal activity which can potentially have a significant adverse affect on the environment. As a consequence, a model for predicting dispersion of rocket exhaust effluents into the atmosphere was developed under two concurrent contracts for use by the National Aeronautics and Space Administration. The model is intended to identify those situations in which concentrations of toxic exhaust products exceed allowable standards and to provide additional basis for developing launch constraints so that such situations have a minimum probability

of occurring. A description of the model (hereinafter referred to as the MSFC (Marshall Space Flight Center) Multilayer Diffusion Model) with accompanying sample predictions is contained in references 2 and 3. A subsequent revision and simplification of the model appears in reference 4.

Predicting turbulent atmospheric diffusion is at best uncertain, as a review of the state of the art would indicate (refs. 5, 6, and 7). Except for very simple cases of continuous emission over relatively short distances and times, for which Gaussian theory is well established, there is a paucity of experimental data for validating diffusion models. Dispersion of rocket exhaust effluents is a much more complicated problem and is of concern for vertical and horizontal scales of the order of 1 kilometer to 100 kilometers, respectively, and time scales of several hours. Obviously, meteorological conditions vary during this period. Furthermore, the source strength and position vary as functions of time.

The MSFC Multilayer Diffusion Model assumes steady-state Gaussian dispersion. Application of this model for rocket launches requires knowledge of a large number of source and meteorological parameters. Values of many of these parameters are uncertain and must be arbitrarily assumed or empirically determined from experimental data.

In view of the uncertainties regarding the present use of this model and the inadequacies of diffusion models in general, the present investigation was undertaken to conduct parametric studies in an attempt to place bounds on some of the uncertainties of predictions of ground-level concentrations of exhaust effluents resulting from rocket launches at Kennedy Space Center. An additional purpose is to evaluate the effect of more realistic energy addition to the ground-cloud-rise equations used in references 2 to 4 and to introduce a more realistic chemical composition for the stabilized cloud.

The multilayer diffusion model represents a description of gaseous and particulate clouds that grow and disperse in the atmospheric mixing layer above the Earth's surface. The clouds drift along the mean wind direction and are assumed to be closely coupled to the turbulence level and local meteorology in the mixing layer. Figure 1 depicts the evolution and growth of a typical ground cloud. Within about a minute after the rocket has been fired, the ground cloud forms and, because of its initially high temperature, begins rising and commences its drift along the wind. Within a period typically 2 to 5 minutes after rocket-motor ignition the ground cloud reaches an altitude at which it is in buoyant equilibrium with the surrounding ambient air. At this point the cloud is described as being stabilized. At the point of stabilization, the multilayer diffusion model is introduced with the appropriate input parameters and boundary conditions. As the cloud drifts downwind, the cloud centroid remains at a fixed stabilization altitude but the cloud disperses in a three-dimensional manner. The lateral and alongwind concentration distributions of effluents within the cloud are assumed to be Gaussian. The reasoning that underlies such

an assumption is discussed in references 5 and 6. Cramer, reference 8, developed diffusion equations that utilize standard deviations of wind azimuth angle and wind elevation angle. Appropriate values for the diffusion parameters were measured with bidirectional wind vanes over relatively smooth prairie land and reported in references 9 and 10. The Gaussian diffusion model has not been validated for the large-scale, nearly instantaneously formed clouds that result from rocket launches. The mechanical and thermal behavior of these hot, buoyant ground clouds may depart significantly from a Gaussian representation. The scale of turbulent fluctuations in the surface mixing layer that disperses these large clouds can be expected to be quite different from the scale effective in dispersing the smaller clouds that were used initially to test the Gaussian theory (refs. 5, 9, and 11). Until extensive experimental studies are completed, such a model can only be used subject to appreciable uncertainty regarding the predictions of ground-level concentration and dosage patterns. It therefore seems appropriate to investigate some of the uncertainty concerning the model input quantities. The model, as developed from steady-state gradient transport theory for Fickian diffusion, cannot deal rigorously with chemical kinetic behavior or heterogeneous reactions that are strictly time dependent. In addition, time-varying meteorological conditions can only be introduced in a stepwise fashion that is not physically representative of atmospheric behavior. Finally, the assumed vertical distribution of exhaust products within the cloud is of concern because ground-level concentrations from the Gaussian model are known to be sensitive to height variation of the source.

The uncertainties to be studied regarding the present use of the diffusion model deal both with the input conditions as well as with the parameters that describe the diffusion mechanism. Five areas of concern are the following:

1. A large amount of turbulent energy is present as the motor exhausts effluents into the forming ground cloud. This fact could significantly influence both the ground-cloud chemical composition and chemical species distributions.

2. Because of the large number of chemical species present in the plume of solid-rocket motors and because of the high jet temperatures, large uncertainty exists regarding the chemical kinetic behavior in the plume. Substantial afterburning of carbon monoxide would change the composition as well as introduce a large additional amount of thermal energy into the cloud.

3. The correct dependence of the Gaussian model on meteorological variables has not been proven for nearly instantaneous large-scale releases. Also, the diffusion coefficients are obtained from a particular set of meteorological measurements and at best are only approximations to the conditions present within the ground cloud.

4. The lateral, alongwind, and vertical distributions of gaseous species, particulates, and aerosols are not known and must be assigned, a priori, a fixed composition at cloud

stabilization. Model options can be employed to account for gravitational deposition of particulates and also precipitation scavenging after cloud stabilization.

5. The mathematical consequences of dividing the lower atmosphere into layers are not understood. It seems possible that considerable variation in the predictions could result from a different choice for the number of layers comprising the lower atmosphere.

SYMBOLS

C_H	effective heat release from rocket motor, cal/gm of propellant
c_p	specific heat of air at constant pressure, cal/gm K
H_m	height of mixing layer, meters
L	alongwind cloud length defined by equations (11), meters
P	Gaussian probability integral
$\tilde{P}$	normalized Gaussian probability integral, $P\sqrt{2\pi}$
p	pressure, mb
Q_I	effective heat release into cloud, cal
Q_K	rocket-exhaust source strength, ppm-m^2
r_K	cloud radius in Kth layer, meters
r_R	initial cloud radius, meters
T	temperature, K
t	time, sec
t^*	time of layer transition from sublayer structure to single layer structure in surface mixing layer, sec
U	mean windspeed, m/sec

U_{RK} windspeed at reference height, m/sec

ΔU windspeed change, m/sec

$\Delta U_{(L>1)}$ windspeed shear in $L > 1$ layer, m/sec

$\Delta U_{(L=1)}$ windspeed shear in $L = 1$ layer, m/sec

V_K volume of each layer segment of cloud

x distance from point of cloud stabilization along mean wind, meters

y lateral distance measured normal to mean wind direction, meters

Z height, meters

Z' height of midpoint of a layer $\frac{Z_{BK} + Z_{TK}}{2}$, meters

Z_{mI} ground-cloud stabilization height, meters

Z_{RK} reference height of 2 meters

z vertical distance measured from local ground level, meters

α lateral diffusion exponent

β vertical diffusion exponent

γ empirical ambient air entrainment coefficient

θ mean wind direction, deg

$\theta'_K = \left(\theta_{TK} + \theta_{BK}\right)\frac{\pi}{360}$

$\theta'_L = \left(\theta_{TL} + \theta_{BL}\right)\frac{\pi}{360}$

ρ ambient air density, gm/m^3

$\sigma = \frac{\gamma Z_{mI}}{2.15}$ standard deviation of cloud source dimension at Z_{mI}, meters

σ_A standard deviation of wind azimuth angle, deg

σ_{AR} standard deviation of wind azimuth angle at reference height, deg

σ_E standard deviation of wind elevation angle, deg

σ_{ER} standard deviation of wind elevation angle at reference height, deg

σ_{xo} standard deviation of alongwind distribution at source, meters

σ_{yo} standard deviation of crosswind distribution at source, meters

σ_{zo} standard deviation of vertical distribution at source, meters

σ_{XLK} standard deviation of alongwind concentration distribution in Lth layer, meters

σ^*_{XK} standard deviation of alongwind dosage distribution in Kth layer at time t^*, meters

σ^*_{YK} standard deviation of crosswind dosage distribution in Kth layer at time t^*, meters

τ_K cloud-stabilization time, sec

τ_{oK} sampling time for standard-deviation calculations, sec

Φ potential temperature $\left[T\left(\frac{1000}{p}\right)^{0.286}\right]$

χ concentration of an effluent at ground level, ppm

χ_K concentration of an effluent in Kth layer, ppm

Subscripts:

BK bottom of Kth layer

TK top of Kth layer

BL bottom of Lth layer

TL top of Lth layer

PARAMETER VARIATIONS

Variation of the most significant parameters affecting the model predictions will be carried out in a nearly independent manner. The unresolved questions regarding the model dependence on meteorological parameters lessens the value of a fully dependent sensitivity analysis at the present time. The parameter variations investigated span a range of plausible cloud and rocket-motor characteristics such that realistic limits of uncertainty can be set regarding the model predictions.

The following table summarizes the range of multilayer-diffusion-model parameter variations studied in the present work:

Lateral diffusion exponent, α . . . . . 0.5 to 1.5
Vertical diffusion exponent, β . . . . . 0.5 to 1.5
Source strength in each layer, Q_K, ppm-m^2 . . . . . 10^3 to 2×10^7
Source-strength distribution in each layer, Q_K, ppm-m^2 . . . . . Uniform; Gaussian; step function
Mixing-layer division (layer grid spacing), K . . . . . 7 layers to 28 layers
Stabilized cloud geometry . . . . . Right circular cones; right circular cylinders: both with equal volumes, with and without equal mass loadings
Specific energy release from rocket motor, C_H, cal/gm . . . . . 690 to 2980
Meteorology . . . . . Low-level sea-breeze regime; fall fair-weather regime at Kennedy Space Center
Mixing-layer depth, H_m, meters . . . . . 300 to 750

Tables I and II list the diffusion-model input values for a low-level sea-breeze meteorological regime and a fall fair-weather regime at Kennedy Space Center.

The principal constituents of present-day solid-rocket motors are typified by the Titan III zero-stage and the Castor II solid-motor compositions. The exit-plane chemical species mass fractions are summarized in reference 4. For the Titan III zero stage the major propellant mass fractions are as follows:

H_2O	H_2	N_2	CO	CO_2	HCl	Al_2O_3	$FeCl_2$	NO
0.068	0.025	0.084	0.280	0.028	0.207	0.304	0.004	0.00021

The zero-stage mass flow rate is 4.17×10^6 gm/sec. Because the atmospheric diffusion mechanism is assumed to be the same for all of the constituent gases, only one gas, HCl, has been dealt with in detail in the present study. There is considerable uncertainty regarding the heterogeneous reactions involving aluminum, and proper treatment of any aluminum-oxide particulate matter in the diffusion mechanism requires presently unknown size and number density distributions as well as an understanding of the chemical and physical behavior of the aluminum oxide.

Initial Mass Distributions and Cloud Geometry

There is insufficient evidence at present to support a particular choice for the distribution of chemical species within the stabilized ground cloud. The kinetic energy of the propellants at the motor exit plane suggests an initially well mixed ground cloud. A characteristic time required to produce a nonuniform concentration distribution in the cloud has not been determined as yet. The size distribution of Al_2O_3 particles will most certainly influence the particle distribution and settling rates. Since knowledge of the particle size distribution and the state of HCl in the cloud is lacking, these constituents have been treated as gases for the majority of calculations reported in references 2 to 4. In order to distribute the exhaust products within the cloud, a given chemical and physical composition must be assumed at cloud stabilization, as well as lateral, alongwind, and vertical distributions of the exhaust products within the cloud. To allow for vertical distribution of material, the cloud is divided vertically into a layered structure with layer boundaries placed at major changes or discontinuities in temperature, windspeed, and wind direction. Turbulent mixing is assumed not to occur across these layer boundaries. The distribution of exhaust material in each layer is assumed to be uniform with the overall vertical mass distribution in the cloud chosen as either uniform or Gaussian. The visible edge of the cloud is assumed to be located where the concentration has fallen to 10 percent of the value along the cloud vertical center line.

The layer structure assumed at the point of cloud stabilization can be replaced at an arbitrary point downwind by a new layer structure that in principle accounts for a mixing-layer meteorology that differs from the conditions that existed at the location of stabilization. This mechanism is termed layer transition, and by employing model 4 option (ref. 4) turbulent mixing can be allowed in the model over the entire depth of the surface mixing layer. There are six model options that can account for an assumed ellipsoidal cloud geometry as well as gravitational settling of particulates and precipitation scavenging out of the ground cloud. The majority of work reported to date has made use of the model 4 option. The present study is primarily concerned with the model 4 option.

Some insight into the different ground-level predictions can be obtained by variation of the vertical distribution of mass in the cloud. The exhaust products have typically been

introduced as having a Gaussian mass distribution or a uniform vertical mass distribution. For model 4 option the Gaussian mass distribution has been reported primarily in connection with a cloud geometry that approximates two right circular cones base to base. This assumed geometry can be obtained from the following formulas for the cloud radius:

$$r_K = \gamma Z' \qquad \text{for} \begin{cases} Z' \leq Z_{mI} \\ r_R = 0 \end{cases} \tag{1}$$

$$r_K = \gamma\left(2Z_{mI} - Z'\right) \qquad \text{for} \begin{cases} Z' > Z_{mI} \\ r_R = 0 \end{cases} \tag{2}$$

where

$$Z' = \frac{Z_{BK} + Z_{TK}}{2} \tag{3}$$

These equations describe the cloud as being contained within two right circular cones whose bases are located at the stabilization height, Z_{mI}. Figure 2 is a diagramatic repre sentation of such a cloud. For a Gaussian vertical mass distribution, the mass fraction in each layer, F_K, of the total mass of a constituent that is in the entire cloud is given by the following:

$$F_K = \frac{Q}{\sqrt{2\pi}} \int_{-\infty}^{\omega} e^{-0.5\omega^2} d\omega \qquad \text{for} \quad K = 1 \tag{4}$$

where Q is the total mass of a constituent in the cloud and is equal to τ_K (mass flow rate) (motor mass fraction of chemical constituent),

$$\omega = \frac{Z_{TK} - Z_{mI}}{\sigma} \tag{5}$$

and

$$\sigma = \frac{\gamma Z_{mI}}{2.15} \tag{6}$$

From reference 4

$$F_K = \frac{Q}{\sqrt{2\pi}} \left[\int_{-\infty}^{\omega} e^{-0.5\omega^2} d\omega - \int_{-\infty}^{\omega'} e^{-0.5(\omega')^2} d\omega' \right] \quad \text{for} \quad K > 1 \tag{7}$$

where

$$\omega' = \frac{Z_{BK} - Z_{mI}}{\sigma} \tag{8}$$

The relationship between the volume of each layer segment of the cloud, V_K, and the Gaussian integrals for vertical mass distribution are shown in figure 3. Both the volume ratio and the Gaussian integrals have been smoothly faired in this figure. The volume ratio, V_K/V_T, where V_T is the total cloud volume, has been normalized by a constant K_1 to yield a value of unity in the layer containing the cloud centroid, and the Gaussian integrals have been normalized by multiplying by the value $\sqrt{2\pi}$. Figure 3 shows the nonlinear relationship between cloud volume change with altitude and the Gaussian integral functions for mass distribution. Figure 4 is a plot of the smoothly faired ratio, $\frac{K_1 V_K/V_T}{\tilde{P}}$, as a function of altitude. It is seen that the volume ratio in the lower portions of the cloud is as much as a factor of two greater than the normalized Gaussian function. Figure 4 indicates that the vertical concentration distribution in the cloud is not Gaussian. For values of the ratio $\frac{K_1 V_K/V_T}{\tilde{P}}$ less than unity, the concentration will be greater than a Gaussian distribution and, for values of this ratio greater than unity, the concentration will be less than a Gaussian distribution. The diffusion model contains the assumption that the mass distribution in each layer of the cloud is uniform over the layer so that the actual concentration distributions will appear as step functions from one layer to the next. No unique cloud geometry or cloud mass distributions have been found to date. The effects of a different geometry and mass distribution are part of the present study.

Lateral and Vertical Diffusion Coefficients

In previous calculations using the present diffusion model (refs. 3 and 4) the lateral diffusion exponent, α, and the vertical diffusion exponent, β, have always been assigned a value of unity. It is believed that these two exponents are not equal and in fact vary over a range of values under different meteorological conditions. (See ref. 5.) The correct physical representation of the crosswind cloud growth is strongly dependent on α. Alternatively, the ground-level concentrations are strongly dependent on the cloud geometry so that a principal element of interest in the present work is the variation of cloud growth and concentration at ground level with realistic changes in the lateral diffusion coefficient. In addition, the alongwind cloud growth is dominated by windspeed change. For low values of windspeed change, the alongwind growth is very limited and only small changes from the original stabilized cloud size are calculated. These effects are investigated in the present work.

Cloud Rise With and Without Afterburning of Carbon Monoxide

The cloud-rise formulas adapted from the work reported in reference 12 provide for a conservation of vertical momentum due to buoyancy of the hot ground cloud. The altitude at which the cloud stabilizes is dependent on the potential temperature gradient through the mixing layer and also on the total heat release from the motor and resulting chemical reactions. For a stable atmosphere the stabilization height as published in reference 4 was derived from a conservation of vertical momentum and buoyancy forces. The cloud centroid stabilization height is given by

$$Z_{mI} = \left[\frac{6Q_I}{\pi \rho c_p \gamma^3 \frac{\partial \Phi}{\partial z}} + \left(\frac{r_R}{\gamma} \right)^4 \right]^{1/4} - \frac{r_R}{\gamma} \tag{9}$$

The present disparity in accepted values for Q_I is partly due to the uncertainty regarding carbon monoxide afterburning. Complete afterburning would add about 1370 cal/gm to the currently accepted value for heat release of 1610 cal/gm for solid motors like the Castor II motors. The variations in stabilization heights with and without afterburning are outlined in this study.

Layer Division of the Atmosphere

No reported studies have been made regarding the possible mathematical consequences of dividing the surface layer at temperature and windspeed and direction discontinuities. The coarse layer structure that invariably results could conceivably introduce significant truncation-like errors into the calculation. Conversely, with an extremely fine layer structure the turbulent mixing would tend to be severely damped and limits that do not appear physically reasonable would be imposed upon the scale of turbulent motion which might invalidate the physical representation of atmospheric processes. The present work delineates some of these effects.

Limiting Meteorological Regimes

Large changes in ground-level predictions can occur due to different meteorological regimes. For the present study two characteristic weather patterns for Cape Kennedy were utilized. One is documented as a low-level sea-breeze regime and the other is typical of fall fair weather. See figures 5(a) and 5(b) for the temperature, wind direction, and windspeed variation with altitude for these two regimes. The primary factor affecting different ground-level predictions between these two weather patterns is the height of the temperature inversion above ground. For fall conditions the centroid of the ground cloud is calculated to stabilize at an altitude close to 1.1 kilometers. Thus, extensive cloud expansion is allowed prior to stabilization. For the low-level sea-breeze regime, the

cloud stabilizes at an altitude near 0.6 kilometer and the growth of the cloud is strongly resisted, giving rise to high predicted ground-level concentrations.

Layer Transition

In order to distribute exhaust products vertically, an initial layered structure can be chosen for the surface mixing layer. To accommodate a change in meteorological conditions and/or turbulent diffusion across the original layer boundaries, the model has been developed with a layer breakdown capability (model 4 option). At an arbitrarily specified time after launch, the layer structure originally assumed may be discarded, a new set of input values calculated, and a new layer structure employed. With the new structure, turbulent mixing can occur over a larger vertical dimension than with the original layer structure. Values of 1 second after cloud stabilization have been used exclusively in the past for model studies. The effect of other choices for the time of layer breakdown will be investigated.

Chemical Composition of the Stabilized Cloud

In order to determine the correct source-term inputs to the model, a correct representation of the cloud composition is imperative. At present the size distribution and number density of Al_2O_3 particles is under intensive study (ref. 13) as is the ultimate state and distribution of HCl. Of interest for the present work is an estimate of the time scale and completeness of carbon-monoxide afterburning. A Delta booster (Castor II motor) exhaust-plume calculation was made using the finite-rate, turbulent, rocket-plume program reported in reference 14. The eddy-viscosity model reported in reference 15 was used. The results and implications from these calculations are presented.

RESULTS

Variation of Source Distributions

The choice of stabilized cloud geometry is, for the most part, arbitrary. The ground-level concentrations, however, are strongly dependent on what stabilized cloud shape is chosen and how the mass is assumed to be distributed within the cloud. The results of choosing a different cloud geometry have been studied in conjunction with variations in the mass loading within the cloud. Recalling equations (1) and (2), it is possible to choose an alternative geometry for the stabilized cloud that conforms to a cylindrical cloud. This choice can be interpreted as resulting from cylindrical entrainment of ambient air with an effective cloud radius and vertical dimension that produce a total cloud volume equal to the conical cloud that has been used in references 3 and 4. Alongwind and crosswind Gaussian distributions can be preserved in the cylindrical cloud with arbitrarily chosen vertical mass distributions. Several important effects can be studied

by this variation of cloud geometry. The difference in ground-level concentrations and dosages between conical and cylindrical clouds can be studied, and also the effects of variations of the lateral and vertical diffusion exponents on two different clouds can be studied. Figure 6 shows the pertinent dimensions for the Titan III-E conical and cylindrical clouds at stabilization for a low-level sea-breeze meteorological regime at Kennedy Space Center. Titan III-C results would be almost identical to the Titan III-E results.

Figure 7 is a plot of the peak ground-level concentration as a function of alongwind distance from the point of cloud stabilization for HCl from a Titan III-E rocket launch. Figure 8 shows the corresponding peak HCl dosage at ground level. These two plots serve as references for the cases that follow.

In figures 7 and 8, the same total mass of HCl was employed for each cloud geometry. A Gaussian vertical source distribution of mass was chosen for each cloud, and Gaussian alongwind and crosswind distributions were preserved for both clouds.

It is seen that both the conical cloud and the cylindrical cloud fill the surface mixing layer about 8 kilometers downwind from stabilization. The local maximum that appears in these curves near 8 kilometers results when the ground cloud fills the surface mixing layer. Beyond 10 kilometers from cloud stabilization the concentration curves are nearly identical. The dosage curve for the cylindrical cloud is a factor of 1.5 above the conical cloud dosage beyond a distance of 8 kilometers from the launch pad. The divergence of the predicted concentration and dosage curves from about 8 kilometers upwind to 1 kilometer should be expected. The conical cloud extends to the ground at stabilization and can diffuse HCl downward initially from the point of stabilization. The cylindrical cloud has virtually no HCl at ground level at the time of stabilization. This result is not unlike the ellipsoidal cloud case reported in reference 4. Although the concentration and dosage plots are carried out starting from 0.5 kilometer from cloud stabilization downwind to 100 kilometers, it should be appreciated that the cloud travels typically 1 to 4 kilometers downwind from launch before reaching a stabilized altitude. Upwind of the point of cloud stabilization the diffusion model as presently established cannot give meaningful results; that is, diffusion to the ground of toxic fuel would be occurring with the cloud centroid at an altitude less than the stabilization altitude. For the conical clouds the implication is that the lower tip of the cloud never rises above the surface, and thus substantial HCl concentrations would exist all the way from the launch pad downwind to cloud stabilization. However, the model cannot be used in the near field between the launch pad and cloud stabilization. The physical justifications for studying such distributions are the following:

1. Heavy Al_2O_3 particles from the rocket exhaust may exhibit a high density distribution in the lower portions of the cloud. Because of the possibility that HCl has chemically or physically combined with the Al_2O_3 particles, the HCl mass distribution could well be higher in the lower portions of the cloud.

2. Several Titan III ground clouds have retained massive amounts of exhaust products near ground level. Significant variations in the vertical mass loading of such clouds must be accounted for by any diffusion model. As an indication of this behavior, figures 9(a) to 9(d) show tracings of a Titan III cloud at Vandenberg Air Force Base. These tracings were taken from actual photographs (unpublished). Figures 10(a) to 10(c) are previously unpublished photographs of a Titan III cloud at Kennedy Space Center. No times were obtainable from these photographs; however, the low-altitude portions of the cloud are apparent. If the distribution of HCl is not symmetrical in the vertical direction about the cloud centroid, then a comparison of the effects of such nonsymmetry is of importance, particularly with regard to different cloud geometries. Figure 11(a) is a plot of the ground-level HCl concentrations that result using the source terms shown in the figure with a conical cloud geometry. Figure 11(b) is a similar plot for a cylindrical cloud geometry. Several interesting results are apparent. Both cloud geometries produce peak concentrations that move downwind at nearly identical locations as the peak mass loading of the cloud is moved upward from the lowest layer (K = 1) of the cloud. These figures indicate that both cloud geometries fill the surface mixing layer at equal values of distance alongwind. This result is not surprising, as the diffusion mechanism remains the same for both clouds. Large differences in ground-level predictions result from the mass-loading variations shown. Also, the alongwind distance at which the peak concentrations lie varies from a point at which the cloud stabilizes to about 9 kilometers from the point of cloud stabilization. Even with similar vertical diffusion within the two cloud geometries, the conical cloud results in as much as a factor of eight greater ground-level concentrations of HCl than the cylindrical cloud at downwind distances greater than 100 kilometers. This result is difficult to accept considering that a smaller total mass of HCl was initially distributed in the conical cloud than in the cylindrical cloud for the particular cases shown in figures 11(a) and 11(b). Figure 12 combines the results of figures 11(a) and 11(b) for comparison.

3. Penetrations of a Titan cloud on May 30, 1974 (unpublished) have indicated that the upper half of the cloud was well mixed and remained so up to t + 34 minutes, at which time the sampling aircraft ceased making penetrations.

Most of the predictions reported in references 3 and 4 have been made utilizing the conical cloud geometry illustrated in figure 6 with the assumption of a Gaussian mass distribution in the vertical direction. Figure 13 shows a comparison of the HCl concentration that results from the Gaussian conical cloud and a uniformly distributed mass of HCl within a cylindrical cloud. The total HCl mass loading from the Titan III-E is conserved between the two clouds. The pertinent diffusion coefficients and layer transition times are shown in the figure. Figure 13 typifies the large uncertainty in ground-level predictions of toxic fuels that results from present ignorance of the correct source distributions and geometry for the stabilized ground cloud.

Cloud Growth and Variations of the Diffusion Exponents

As might be anticipated, variation of the lateral diffusion exponent, α, produces strikingly different effects on the two different cloud geometries. Figure 14 shows the predicted ground-level HCl concentrations for the conical cloud over a range of values for the lateral and vertical diffusion exponents, α and β. Differences between the HCl concentrations of as much as a factor of 10 exist as far downwind as 100 kilometers for the range of exponents used in this figure. A principal reason for varying these coefficients is to compare the concentration predictions for a given set of α and β values and the effect on the predicted cloud growth alongwind and across the wind. The diffusion model as reported in references 3 and 4 has employed exponents of unity for α and β. The result for several characteristic meteorological conditions at Kennedy Space Center is a cloud that is predicted to grow to enormous dimensions across the wind but to remain almost constant in the alongwind dimension. This behavior has not been observed experimentally from photographic studies of ground clouds, and thus the validity of the present characterization of the cloud growth is of concern. It is possible that the values of α and β are substantially different from the previously assumed value of unity. The parameters α and β are exponents in the cloud expansion terms. Figure 15 is an example of the variation in predicted alongwind and crosswind cloud growth for two sets of values for α and β. (See the appendix for cloud growth dependence on α and β.) These curves were obtained from calculations for a Titan III-E ground cloud during a low-level sea-breeze regime at Kennedy Space Center. Values of α chosen larger than unity seem totally unreasonable. Even for a value of α of 0.5 the crosswind cloud dimension is four times the alongwind dimension at 100 kilometers downwind. The diffusion model representation of alongwind cloud growth must be questioned. The standard deviation of the cloud alongwind concentration distribution is given as

$$\sigma_{XLK} = \left\{\left[\frac{L(X_{LK})}{4.3}\right]^2 + \sigma^{*2}_{XLK}\right\}^{1/2} \tag{10}$$

where

$$\left.\begin{aligned} L(X_{LK}) &= 0.28\left(\frac{\Delta U}{U}\right)X_L \qquad \text{for} \quad \Delta U > 0 \\ L(X_{LK}) &= 0 \qquad\qquad\qquad\quad \text{for} \quad \Delta U \leqq 0 \end{aligned}\right\} \tag{11}$$

and

$$\sigma^{*}_{XLK} = \left\{\left[\sigma^{*2}_{XK}\cos^2\left(\theta'_K - \theta'_L\right)\right] + \left[\sigma^{*2}_{YK}\sin^2\left(\theta'_K - \theta'_L\right)\right]\right\}^{1/2} \tag{12}$$

These equations show that for zero or negative values of windspeed change, ΔU, the alongwind cloud growth depends weakly on the angle $\theta'_K - \theta'_L$. The alongwind cloud growth is assumed independent of any diffusion mechanism comparable to the crosswind diffusion. The alongwind cloud growth given by

$$L = 0.28 \frac{\Delta U x}{U} \tag{13}$$

was derived by Tyldesley and Wallington (ref. 11) from theoretical considerations for the diffusion of plumes and crosswind line sources. The alongwind diffusion coefficient was taken as zero. In the case of zero or negative values of windspeed change, these results cannot be derived and, in fact, alongwind diffusion cannot be neglected. In addition, it is difficult to argue that the cloud will be dependent on positive values of windspeed shear but independent of negative values of windspeed shear. Equations (10) to (12) do not produce alongwind cloud growths with dimensions that compare with the calculated crosswind growth or with experimentally observed rocket-generated ground clouds. Because the ground-level predictions are strongly affected by the assumed cloud-growth mechanism, this problem must be resolved if a major uncertainty in the diffusion model is to be overcome. An extreme example occurs for the Titan III-E ground cloud during a low-level sea-breeze meteorological condition at the Kennedy Space Center. The windspeed change is negative above an altitude of 300 meters, and the alongwind cloud dimension is predicted to remain constant for more than 100 kilometers downwind. The crosswind dimension, however, grows to more than 100 times the alongwind dimension.

Figure 16 shows a plot of the ground-level HCl concentrations as a function of downwind distance when α and β are varied for a Titan III-E ground cloud assumed to be cylindrical in shape at stabilization with a uniform vertical mass loading in layers 3, 4, and 5. (The visible cloud does not reach the ground at the time of stabilization.) The variation both in the levels of concentration as well as in the location of the peak values is very large. Apparently the same parametric variation of diffusion exponents has a more significant effect on the cylindrical cloud than on the conical cloud. The point of interest here is that the uncertainty due to the assumed values of α and β is strongly dependent on cloud geometry. Figure 17 allows a comparison between conical and cylindrical clouds for two sets of values for the diffusion exponent.

An example of the uncertainty that exists regarding crosswind cloud growth is typified by a comparison between measured and calculated crosswind growth during a Titan III launch at Kennedy Space Center in February 1974 (unpublished). Figure 18 shows the mixing-layer meteorology at launch time. Figure 19 shows calculated cloud crosswind dimensions. Both visible and infrared (IR) images of the cloud were obtained from a camera site almost directly upwind of the cloud path. The measured crosswind cloud dimensions are also shown in this figure. The measured growth is about a factor of four less

than predicted by the diffusion model. This discrepancy would produce a substantial increase in ground-level concentration predictions if the cloud crosswind growth in the model were reduced by a factor of four.

Model Sensitivity to Assumed Time of Change in Atmospheric Layer Structure

Figure 20 shows the model sensitivity to assumed variations in the layer-transition time. At t^* the sublayer boundaries at $K = 1$ to $K = 4$ are removed (for the low-level sea-breeze regime), and turbulent diffusion is allowed over the entire original $K = 1$ to $K = 4$ vertical region. The criteria for determining a correct value for t^* have not been well established. The present study has shown that the ground-level concentration predictions converge to a single solution as t^* approaches zero. This fact lends credence to the concept of a layer-transition capability in the diffusion model. The principal reasons for choosing a layered structure in the atmosphere were to allow a nonuniform distribution of exhaust products in the vertical direction. A second goal of the layer-transition concept is to allow a step-function input of new meteorological conditions to be introduced into the diffusion model. This capability of the model could be an important requirement for modeling diffusion as a ground cloud moved over a land-ocean interface. Thus, for the Cape Kennedy area, layer-transition times on the order of minutes could be required. It can be seen that downwind to about 8 kilometers large differences in the ground-level HCl concentrations result for different values of t^*. For downwind distances greater than 8 kilometers, all of the results are nearly identical. When $t^* > 110$ seconds, the rapid rise in concentration with distance produces solutions that are nearly singular in the region between 0.5 to 1.0 kilometer downwind of cloud stabilization. At a downwind distance of 1 kilometer there is as much as three orders of magnitude difference between the HCl concentrations at ground level depending on the values of t^* that are assumed.

Figure 21 shows the model sensitivity for a cylindrical cloud geometry to variations in the layer-transition time. For downwind distances greater than about 8 kilometers, the cylindrical cloud produces ground-level HCl concentrations nearly identical with those produced by the conical clouds. Upwind of the 8-kilometer location, the cylindrical-cloud results exhibit a greatly reduced variation in HCl concentration with assumed values of t^*. The singularity in the computational scheme occurs very nearly at $t^* = 110$ seconds similar to the conical-cloud results. As formulated, the diffusion model cannot be used for transition times greater than about 110 seconds. From a practical standpoint, there is insufficient spatial resolution of the measured meteorological inputs to the model to allow new inputs to be introduced at large values of layer-transition times. The surface mixing layer is characterized by turbulent dispersion, and it thus seems far more acceptable to choose small values for layer-transition time in order to allow the turbulent dispersion

to take place over the entire cloud contained within the mixing layer as soon after cloud stabilization as possible.

Model Sensitivity to Subdivision of the Layer Structure

The results of subdividing the original layer heights for the Titan III-E conical cloud during a low-level sea-breeze regime are shown in figure 22. The original 7-layer structure was transformed to a 14-layer structure and also to a 28-layer structure with linear interpolation used to obtain the wind field and turbulence parameters at the new layer boundaries. Figure 22 indicates that the 14- and 28-layer models produce ground-level HCl concentrations 2.0 times greater than the 7-layer model over most of the downwind travel of the cloud. This result is a numerical consequence of the model formulation and has little bearing on the actual physical processes tending to disperse the cloud toward the ground. Specifically the layer structure has been arbitrarily chosen at discontinuities in temperature and wind-field parameters. Within the surface mixing layer for large-scale three-dimensional cloud dispersion, this assumption has not as yet been experimentally validated. Figure 23 shows the results for a cylindrical cloud with 7-layer and 14-layer structures. The 14-layer downwind HCl concentrations are about 25 percent below the 7-layer results. It appears that the computational scheme is less sensitive to the cylindrical-cloud mass distribution than it is to the conical-cloud distribution. These results show that changing the layer structure produces a more pronounced disturbance on the conical-cloud computations than on elevated sources such as the cylindrical cloud. The implication here is that the conical-cloud sensitivity stems from the redistribution of mass when the Gaussian integrals are evaluated over 14- and 28-layer structures rather than over a 7-layer structure. The computational results are not greatly affected by finer layer structure per se but indirectly through the Gaussian mass distribution in the vertical direction within the conical cloud.

The choice of a layer structure to distribute exhaust products vertically can be made consistent with the thermal and wind-field variations in the surface mixing layer. This layer structure chosen does not, however, guarantee an accurate solution.

Effect on Ground-Level Predictions of Variations in the Assumed Thermal Energy Released Into the Cloud

Three cases were run for a Titan III-E ground cloud within a low-level sea-breeze meteorological regime. The assumed thermal energy released into the cloud and the corresponding cloud stabilization height are shown in figure 24. Previously used values of C_H = 690 cal/gm for the solid motor were used in the cloud-rise equation of the present study. For C_H = 1410 cal/gm the total heat including the rocket-motor exit-plane kinetic energy was assumed to be released into the cloud. For values of C_H = 2980 cal/gm the

previous value for total heat plus the heat release due to complete combustion of the exit-plane CO was assumed. Also shown in figure 23 is the cloud radius in the xy plane at the stabilization altitude. The ground-level concentrations drop significantly as the cloud stabilization height increases. At the higher altitudes the cloud has expanded more fully and thus diluted itself to a greater extent, and also it takes longer for toxic gases to diffuse downward to ground level. These results are shown in figure 25 for the three cases considered. Figure 25 is typical of the results that are obtained for the different assumed heat-release values.

Calculations for a full-scale Castor II solid motor were made for the chemical nonequilibrium rocket-plume behavior. These calculations were carried out using the turbulent plume program reported in reference 14. Figure 24 shows the mole-fraction variation of CO and CO_2 with dimensionless distance downstream from the Castor II nozzle exit plane. Within relatively few exit-plane diameters the plume center line CO mole fraction as well as the half-radius CO mole fraction have fallen significantly, indicating very effective combustion of CO with molecular oxygen from the ambient atmosphere. Even at 30 exit-plane diameters downstream, the center-line temperature is 2655 K and the CO mole fraction has fallen to 0.024 which is nearly one order of magnitude below the exit-plane value. The conclusion is that essentially all of the exit-plane carbon monoxide will be burned in the plume within a rather short distance behind the motor. The results shown in figure 26 are significant both for the cloud-rise predictions as well as the source terms for the diffusion model. It appears to be inappropriate to neglect the thermal release of energy due to afterburning. In addition, a substantial fraction of the exit-plane kinetic energy must be recovered as thermal energy tending to affect the cloud rise. The predicted carbon-monoxide combustion implies a greatly reduced toxic fuel hazard with regard to CO concentrations at ground level and at all levels within the cloud.

Model Sensitivity to Mixing-Layer Height

The layer transition model (model 4 option) provides for turbulent mixing across the original sublayer boundaries after an assumed layer-transition time. The layer transition is intended to include the sublayers that make up the surface mixing layer. As might be expected, large differences in the ground-level concentrations are predicted for different mixing-layer heights, and thus it is imperative that the correct value for the mixing-layer height be specified. Figure 27 illustrates the effect of layer transition for the sublayers 1 through 8 and 1 through 16 at a time of 1.0 second after cloud stabilization. The results are for a 28-layer model for the Titan III-E in a low-level sea-breeze meteorological regime. The top of the 8th layer is at 350 meters above the ground, and the top of the 16th layer is at 775 meters above the ground. The ground-level HCl concentration for the 1- to 16-layer case is 180 times greater than for the 1- to 8-layer case at a downwind distance of 100 kilometers. Physically these results are due to the smaller

portion of the cloud being diffused downward in the case of the 1- to 8-layer transition. The results are also quite dependent on the cloud stabilization altitude and the assumed Gaussian mass loading of the cloud. A cloud with uniform mass loading in the vertical direction can be expected to show fewer dramatic differences in the ground-level predictions when different sublayer transition heights are assumed. The correct specification of mixing-layer height can only come, at present, from measured quantities during a given meteorological condition at the launch site. The importance of being able to specify accurately the mixing-layer height is illustrated by figure 27 which shows substantial differences in ground-level concentration depending on assumed mixing-layer height.

Ground-Level Concentration Patterns for Two Different Meteorological Regimes at the Kennedy Space Center

As an indication of typical diffusion-model sensitivity to different weather conditions, the low-level sea-breeze results shown previously are compared with calculations made for the Titan III-E with a fall fair-weather meteorological regime. The fall fair weather produces a cloud stabilization height of 1055 meters for a total effective heat release of 1410 cal/gm from the solid-rocket motor boosters. In addition, there is a positive nonzero value of windspeed change from the ground level up through the cloud stabilization height. Figure 5(b) illustrates the temperature and wind-field variations with height for the fall regime. Figure 28 shows the HCl concentration as a function of distance along the wind from cloud stabilization. Both the fall fair weather and the low-level sea-breeze calculations utilized the layer-transition option as well as right circular conical-cloud geometries. The greater cloud stabilization height for the fall regime accounts for the ground-level HCl values being below the low-level sea-breeze values. This result is a fundamental consequence of the cloud expansion during its rise to stabilization. The increasing difference in concentration with downwind distance for these two weather patterns is brought about in part by the cloud alongwind growth with downwind travel for the fall weather. This growth is due to the positive windspeed shear for fall weather. Figure 29 is a plot of cloud alongwind and crosswind diameter with distance for the two weather regimes. The cloud growth is inversely related to the HCl concentrations at ground level and within the cloud. Other meteorological conditions can be expected to produce comparable results depending on the magnitude and sign of wind shear and on the cloud stabilization height.

CONCLUDING REMARKS

The present study with the multilayer diffusion model has quantitatively described some large-scale uncertainties in the ground-level predictions for toxic rocket-motor

effluents. Within several kilometers downwind from cloud stabilization, for a given weather pattern, differences greater than three orders of magnitude exist for the ground-level HCl concentrations from a Titan III-E cloud, depending on what cloud geometry is assumed. Similarly different distributions of toxic gas within the clouds can produce ground-level concentrations that differ by a factor of 30 at a downwind distance of 100 kilometers. The correct stabilized cloud geometry and gas-species distributions within the cloud are presently unknown, and thus a particular set of values can only be assumed. Experiments presently underway can greatly reduce the possible limits that exist for these quantities.

A major concern is the diffusion-model characterization of the alongwind and crosswind cloud growth. The parameter variations used in this study indicate that, for certain meteorological conditions typical of the Kennedy Space Center, unrealistic values of alongwind cloud growth result when there is zero or negative windspeed change between the ground and cloud stabilization height. The inadequacy of the model was traced to the use of previous diffusion theory that cannot be applied under the above wind-field conditions.

The diffusion model was found to exhibit several orders of magnitude difference in the near field ground-level HCl predictions depending on assumed layer-transition times. The steep rise in concentration with downwind distance prohibits solutions from being obtained for transition times greater than about 110 seconds.

The diffusion model was found to be dependent on the assumed layer structure from the stabilized ground cloud. A finer layer structure produced a somewhat lower ground-level concentration of HCl at distances greater than about 10 kilometers downwind from stabilization for cylindrical clouds and a factor of two greater concentration for conical clouds.

Calculations for chemical nonequilibrium rocket-plume behavior for a typical solid-rocket motor indicated effective carbon-monoxide afterburning within about 30 nozzle exit-plane diameters downstream. The heat release due to afterburning causes the cloud to stabilize at a greater altitude than with no afterburning. The thermal recovery of a major fraction of the exit-plane kinetic energy as well as the heat release due to afterburning appears to be physically reasonable; however, measurements are needed for comparison with a cloud-rise theory.

Langley Research Center,
National Aeronautics and Space Administration,
Hampton, Va., February 24, 1975.

APPENDIX

THE MULTILAYER DIFFUSION-MODEL EQUATIONS FOR GROUND-LEVEL CONCENTRATIONS OF ROCKET EXHAUST PRODUCTS

The generalized concentration equation for gaseous exhaust products is given in reference 4 as the product of five terms:

$$\text{Concentration} = (\text{Peak concentration term}) \times (\text{Alongwind term}) \times (\text{Lateral term}) \times (\text{Vertical term}) \times (\text{Depletion term}) \tag{A1}$$

A Cartesian coordinate system is used with the origin at $x = 0$, $y = 0$, and $z = 0$. The mean wind direction is along the x-axis, a normal to the mean wind direction is along the y-axis, and the vertical direction is along the z-axis. The terms in equation (A1) can be expressed by the following:

Peak concentration term

$$PT = \frac{Q}{(2\pi)^{3/2}\sigma_x\sigma_y\sigma_z} \tag{A2}$$

where

Q source strength, grams

σ_x standard deviation of alongwind concentration distribution, meters

σ_y standard deviation of crosswind concentration distribution, meters

σ_z standard deviation of vertical concentration distribution, meters

Alongwind term

$$AT = \exp\left[-\frac{1}{2}\left(\frac{x - Ut}{\sigma_x}\right)^2\right] \tag{A3}$$

where

U mean windspeed, m/sec

t time of cloud travel, sec

Lateral term

$$LT = \exp\left[-\frac{1}{2}\left(\frac{y}{\sigma_y}\right)^2\right] \tag{A4}$$

Vertical term

$$VT = \exp\left[-\frac{1}{2}\left(\frac{H - z}{\sigma_z}\right)^2\right] + \exp\left[-\frac{1}{2}\left(\frac{H + z}{\sigma_z}\right)^2\right] + \sum_{i=1}^{\infty}\left\{\exp\left[-\frac{1}{2}\left(\frac{2iH_m - H - z}{\sigma_z}\right)^2\right]\right.$$

$$\left. + \exp\left[-\frac{1}{2}\left(\frac{2iH_m - H + z}{\sigma_z}\right)^2\right] + \exp\left[-\frac{1}{2}\left(\frac{2iH_m + H - z}{\sigma_z}\right)^2\right] + \exp\left[-\frac{1}{2}\left(\frac{2iH_m + H + z}{\sigma_z}\right)^2\right]\right\} \tag{A5}$$

where

H effective source height, meters

H_m height of top of mixing layer, meters

Depletion term

This term can represent simple decay, precipitation scavenging, and/or gravitational settling. For settling, the term appears as:

$$GT = \exp\left[-\frac{1}{2}\left(\frac{H - \frac{V_s x}{U} - z}{\sigma_z}\right)^2\right] + \exp\left[-\frac{1}{2}\left(\frac{2H_m - H + \frac{V_s x}{U} - z}{\sigma_z}\right)^2\right] \tag{A6}$$

where

V_s settling velocity, m/sec

If a particle-size distribution is employed, equation (A6) is solved for a series of particle settling velocities and the results are superposed for the solution to equation (A1).

To illustrate the cloud-growth dependence on the diffusion exponents, α and β, the following expressions from reference 4 are given for the standard deviations of cloud crosswind and cloud vertical dosage distributions:

$$\sigma_{YK} = \left(\left\{ \sigma'_{AK} x_{rYK} \left[\frac{x_K + x_{YK} - x_{rYK}(1 - \alpha_K)}{\alpha_K x_{rYK}} \right]^{\alpha_K} \right\}^2 + \left(\frac{\Delta\theta'_K x_K}{4.3} \right)^2 \right)^{1/2} \tag{A7}$$

where

σ'_{AK} mean layer standard deviation of wind azimuth angle

x_{rYK} distance over which rectilinear crosswind expansion occurs downwind of ideal point source

x_K downwind distance from source

x_{YK} crosswind virtual distance

$\Delta\theta'_K$ vertical wind-direction shear in Kth layer

α_K lateral diffusion exponent in Kth layer

For vertical cloud growth:

$$\sigma_{ZK} = \sigma'_{EK} x_{rZK} \left[\frac{x_K + x_{ZK} - x_{rZK}(1 - \beta_K)}{\beta_K x_{rZK}} \right]^{\beta_K} \tag{A8}$$

where

σ'_{EK} mean standard deviation of wind elevation angle in Kth layer

x_{ZK} vertical virtual distance

x_{rZK} distance over which rectilinear vertical expansion occurs downwind from ideal point source in Kth layer

β_K vertical diffusion exponent

REFERENCES

1. Boone, F. W.; and Van Vleck, L. D.: Rocket Exhaust Air Pollution Prediction and Verification. Ind. Hyg. J., vol. 25, Sept.-Oct. 1964, pp. 499-506.

2. Record, F. A.; Swanson, R. N.; Cramer, H. E.; and Dumbauld, R. K.: Analysis of Lower Atmospheric Data for Diffusion Studies. NASA CR-61327, 1970.

3. Dumbauld, R. K.; Bjorklund, J. R.; Cramer, H. E.; and Record, F. A.: Handbook for Estimating Toxic Fuel Hazards. NASA CR-61326, 1970.

4. Dumbauld, R. K.; Bjorklund, J. R.; and Bowers, J. F.: NASA/MSFC Multilayer Diffusion Models and Computer Program for Operational Prediction of Toxic Fuel Hazards. NASA CR-129006, 1973.

5. Pasquill, F.: Atmospheric Diffusion. D. Van Nostrand Co., Ltd., c.1962.

6. Slade, David H., ed.: Meteorology and Atomic Energy 1968. U.S. Atomic Energy Commission, July 1968.

7. Mathis, Joe J., Jr.; and Grose, William L.: A Review of Methods for Predicting Air Pollution Dispersion. NASA SP-322, 1973.

8. Cramer, Harrison E.: A Practical Method for Estimating the Dispersal of Atmospheric Contaminants. Proceedings of the First National Conference on Applied Meteorology, American Meteorol. Soc., 1957, pp. 33-55.

9. Cramer, H. E.; Record, F. A.; and Vaughan, H. C.: The Study of the Diffusion of Gases or Aerosols in the Lower Atmosphere. AFCRC-TR-58-239, DDC Doc. No. 152 528, U.S. Air Force, May 15, 1958.

10. Cramer, H. E.: A Brief Survey of the Meteorological Aspects of Atmospheric Pollution. Bull. American Meteorol. Soc., vol. 40, no. 4, Apr. 1959, pp. 165-171.

11. Tyldesley, J. B.; and Wallington, C. E.: The Effect of Wind Shear and Vertical Diffusion on Horizontal Dispersion. Quart. J. Roy. Meteorol. Soc., vol. 91, no. 388, Apr. 1965, pp. 158-174.

12. Briggs, G. A.: Plume Rise. U.S. Atomic Energy Commission, 1969.

13. Rhein, Robert A.: Some Environmental Considerations Relating to the Interaction of the Solid Rocket Motor Exhaust With the Atmosphere: Predicted Chemical Composition of Exhaust Species and Predicted Conditions for the Formation of HCl Aerosol. Tech. Mem. 33-659, Jet Propulsion Lab., California Inst. Technol., Dec. 1, 1973. (Available as NASA CR-136558.)

14. Mikatarian, R. R.; Kau, C. J.; and Pergament, H. S.: A Fast Computer Program for Nonequilibrium Rocket Plume Predictions. AFRPL-TR-72-94, U.S. Air Force, Aug. 1972. (Available from DDC as AD 751 984.)

15. Donaldson, Coleman duP.; and Gray, K. Evan: Theoretical and Experimental Investigation of the Compressible Free Mixing of Two Dissimilar Gases. AIAA J., vol. 4, no. 11, Nov. 1966, pp. 2017-2025.

TABLE I.- DIFFUSION-MODEL INPUT VALUES FOR A LOW-LEVEL SEA-BREEZE METEOROLOGICAL REGIME AT KENNEDY SPACE CENTER

Parameter	Unit	Layer						
		1	2	3	4	5	6	7
Z_{BK}	meters	2	50	300	500	700	1000	1500
Z_{TK}	meters	150	300	500	700	1000	1500	2000
Z_{mI}	meters				639			
U_{BK}	m/sec	2.51	7.9	9.5	5.6	4.0	2.7	2.9
U_{TK}	m/sec	7.9	9.5	5.6	4.0	2.7	2.9	3.1
θ_{BK}	deg	140	145	150	161.5	172.5	190	240
θ_{TK}	deg	145	150	161.5	172.5	190	240	250
Φ_{BK}	K	292.2	293.3	293.6	295.5	297.7	300.6	303.2
Φ_{TK}	K	293.3	293.6	295.5	297.7	300.6	303.2	306
p_{BK}	mb	1013	1000	983	961	937	906	855
p_{TK}	mb	1000	983	961	937	906	855	805
$\sigma_{E_{BK}}$	deg	17.80	5.65	4.71	3.60	2.48	.83	.83
$\sigma_{E_{TK}}$	deg	5.65	4.71	3.60	2.48	.83	.83	.83
$\sigma_{A_{BK}}$	deg	21.5	6.83	5.70	4.36	3.01	1.0	1.0
$\sigma_{A_{TK}}$	deg	6.83	5.70	4.36	3.01	1.0	1.0	1.0
τ_K	sec	199						
τ_{oK}	sec	600						
Z_{RK}	meters	18						
U_{RK}	m/sec	4.5						
σ_{AR}	deg	12						
σ_{ER}	deg	9.9						
σ_{xo} (conical cloud)	meters	22.3	66.98	119	178.6	127.3	93.0	93.0
σ_{yo} (conical cloud)	meters	22.3	66.98	119	178.6	127.3	93.0	93.0
σ_{zo} (conical cloud)	meters	43.30	43.30	57.74	57.74	86.60	144.3	144.3
σ_{xo} (cylindrical cloud)	meters			178.6	178.6	178.6		
σ_{yo} (cylindrical cloud)	meters			178.6	178.6	178.6		
σ_{zo} (cylindrical cloud)	meters			57.74	57.74	86.60		

TABLE II.- DIFFUSION-MODEL INPUT VALUES FOR A FALL FAIR-WEATHER METEOROLOGICAL REGIME AT KENNEDY SPACE CENTER

Parameter	Units	Layer									
		1	2	3	4	5	6	7	8	9	10
Z_{BK}	meters	2	200	400	600	800	1000	1200	1400	1600	1800
Z_{TK}	meters	200	400	600	800	1000	1200	1400	1600	1800	2000
Z_{mI}	meters						1055				
U_{BK}	m/sec	3.78	5.97	6.39	6.65	6.85	7.0	6.7	6.45	6.18	5.9
U_{TK}	m/sec	5.97	6.39	6.65	6.85	7.0	6.7	6.45	6.18	5.9	5.6
θ_{BK}	deg	90	95.8	101.6	107.4	113.2	119.0	121.5	124.0	126.0	129.0
θ_{TK}	deg	95.8	101.6	107.4	113.2	119.0	121.5	124.0	126.0	129.0	131.0
Φ_{BK}	K	297.9	298.2	298.6	298.6	299.2	299.0	300.3	301.6	302.9	304.3
Φ_{TK}	K	298.2	298.6	298.6	299.2	299.0	300.3	301.6	302.9	304.3	305.6
p_{BK}	mb	1013	994	972	949	926	906	885	805	844	824
p_{TK}	mb	994	972	949	926	906	885	865	844	824	805
$\sigma_{E_{BK}}$	deg	14.09	9.23	8.61	8.26	8.02	7.85	6.47	5.10		
$\sigma_{E_{TK}}$	deg	9.23	8.61	8.26	8.02	7.85	6.47	5.10	3.73	2.35	
$\sigma_{A_{BK}}$	deg	14.98	9.41	8.78	8.42	8.18	8.00	6.60	5.20	3.80	
$\sigma_{A_{TK}}$	deg	9.41	8.78	8.42	8.18	8.00	6.60	5.20	3.80	2.4	
τ_K	sec	520									
τ_{oK}	sec	600									
Z_{RK}	meters	18									
U_{RK}	m/sec	4.7									
σ_{AR}	deg	12.0									
σ_{ER}	deg	6.6									
σ_{xo}	meters	29.77	89.3	148.8	208.4	267.9	300.0	241.1	181.5	122.0	
σ_{yo}	meters	29.77	89.3	148.8	208.4	267.9	300.0	241.1	181.5	122.0	
σ_{zo}	meters	57.74	57.74	57.74	57.74	57.74	57.74	57.74	57.74	57.74	

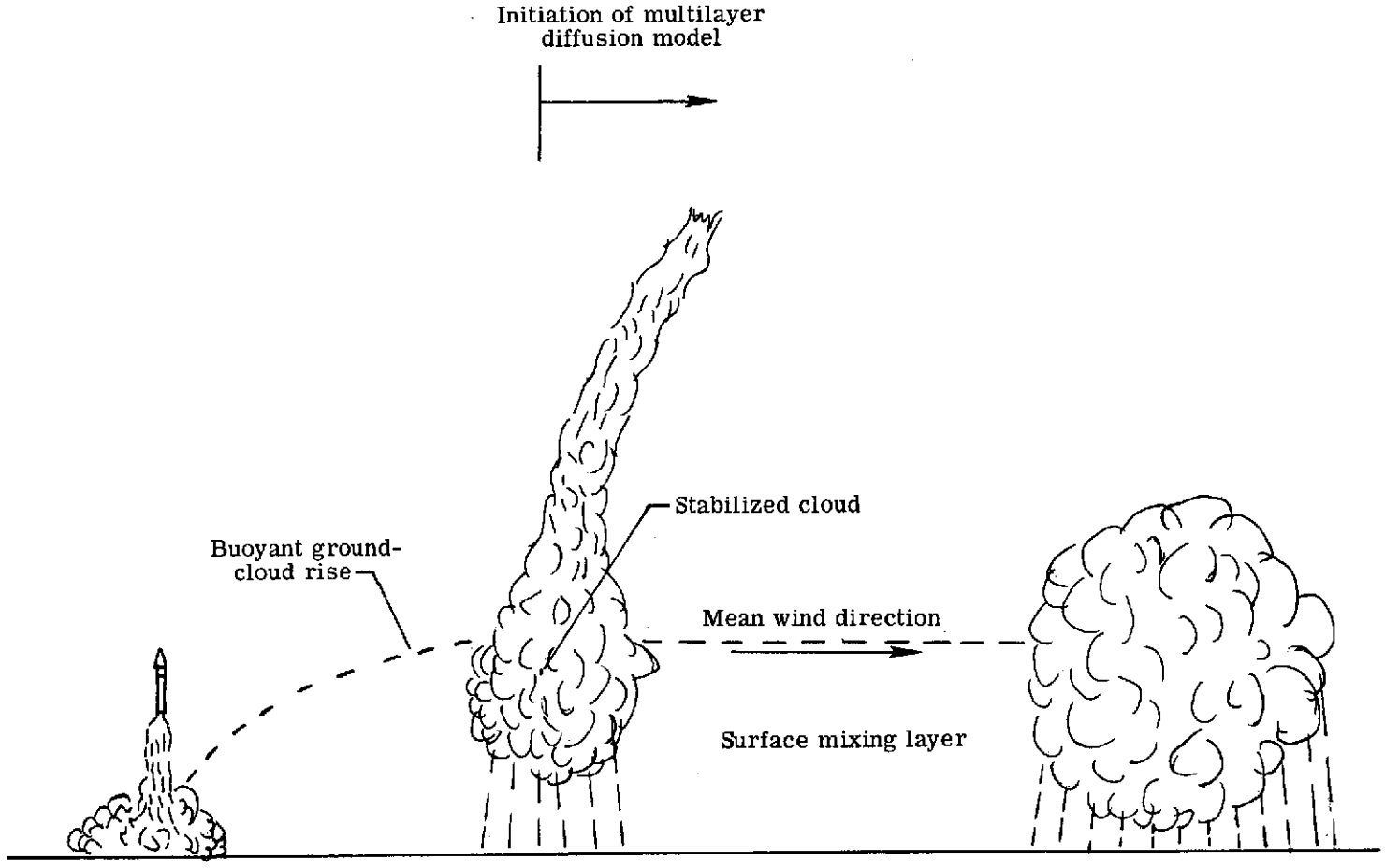

Figure 1.- Schematic diagram of rocket-generated ground-cloud formation, growth, and downwind drift from the launch pad.

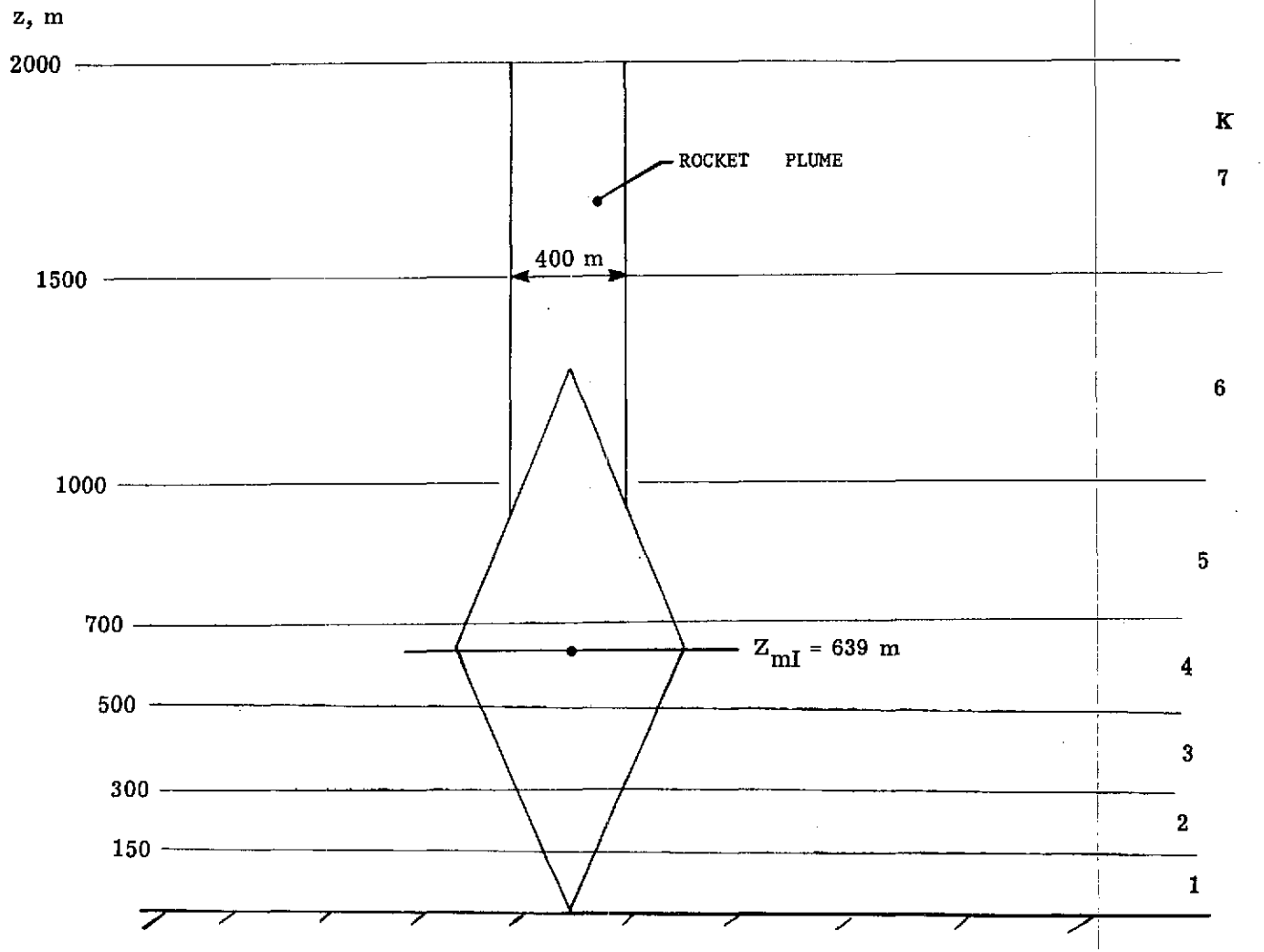

Figure 2.- One assumed geometry of stabilized ground cloud formed by a Titan III-E rocket during a low-level sea breeze at Kennedy Space Center.

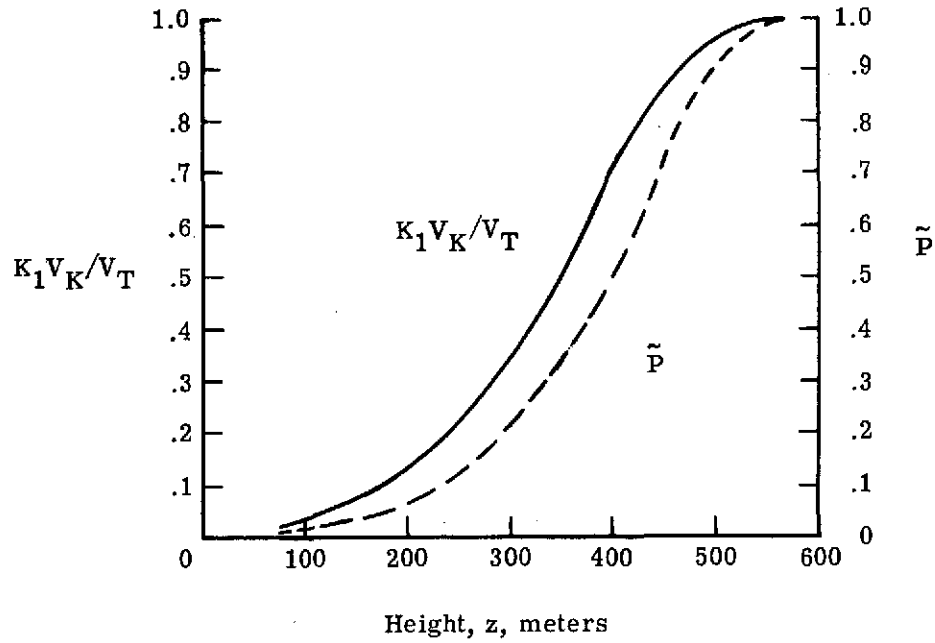

Figure 3.- The relationship between the volume of each layer of a conical cloud and the Gaussian probability integrals for mass distribution in each layer. $K_1 = 1.89$.

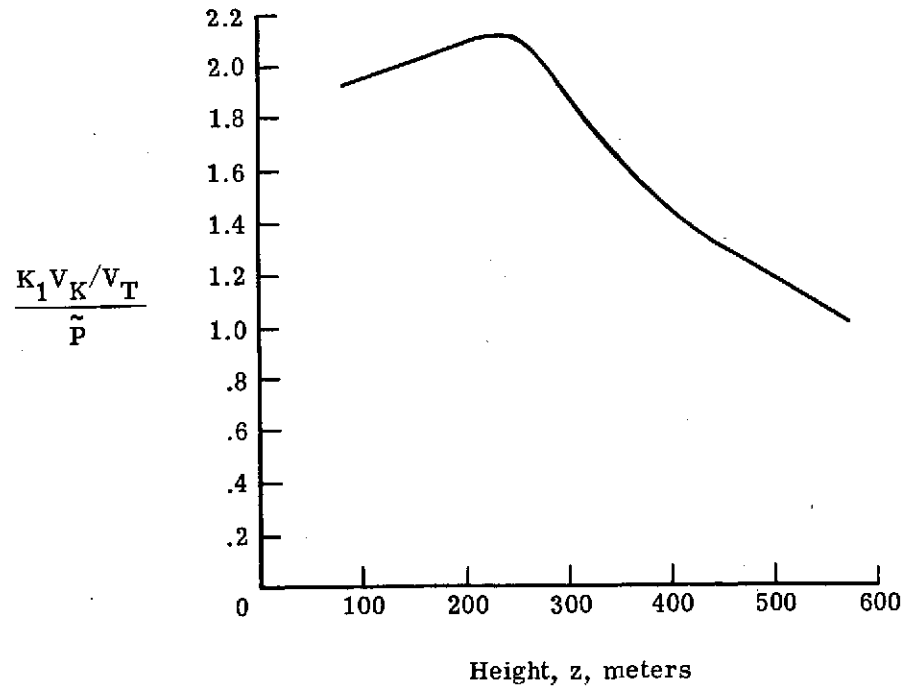

Figure 4.- The ratio of normalized volumes for conical clouds to the Gaussian integrals for mass distribution in the vertical direction.

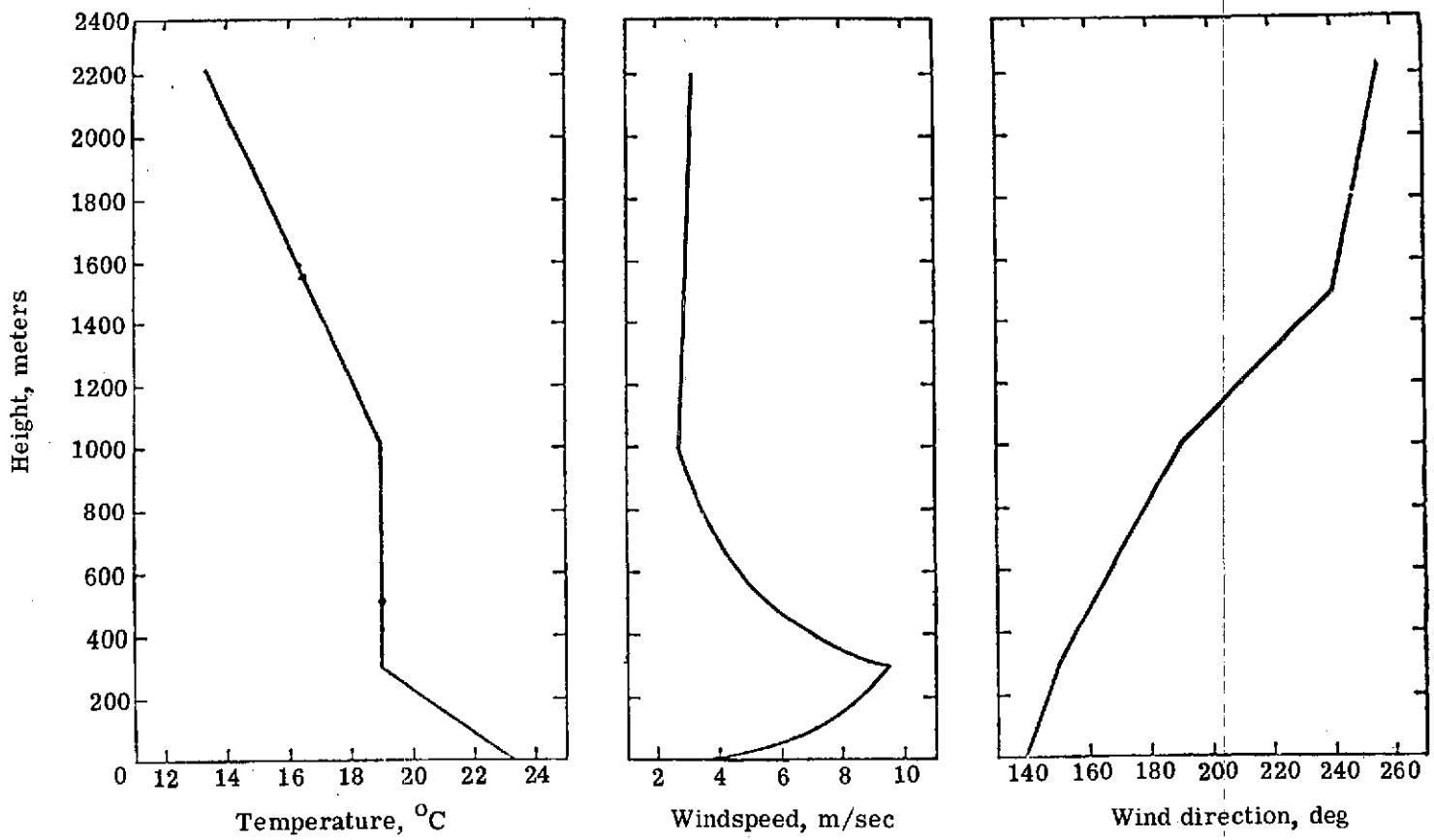

(a) Low-level sea-breeze meteorological regime.

Figure 5.- Variation of ambient temperature, windspeed, and wind direction with altitude at Kennedy Space Center.

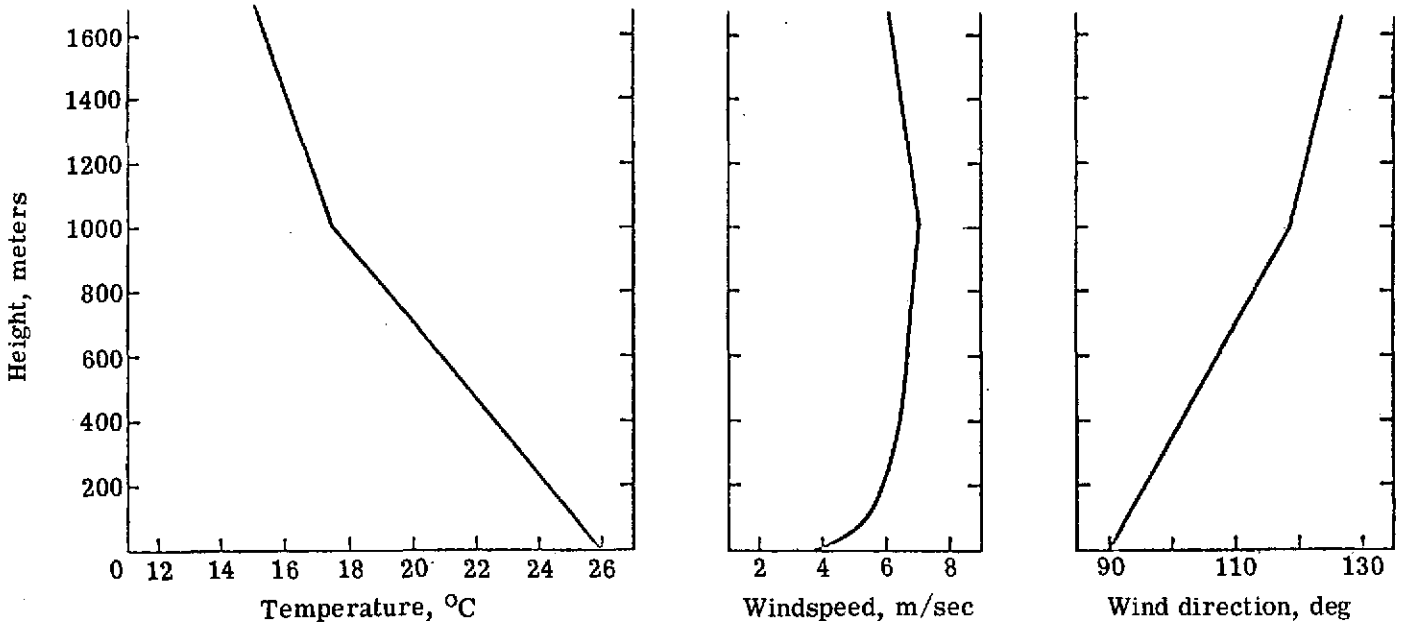

(b) Fall fair-weather meteorological regime.

Figure 5.- Concluded.

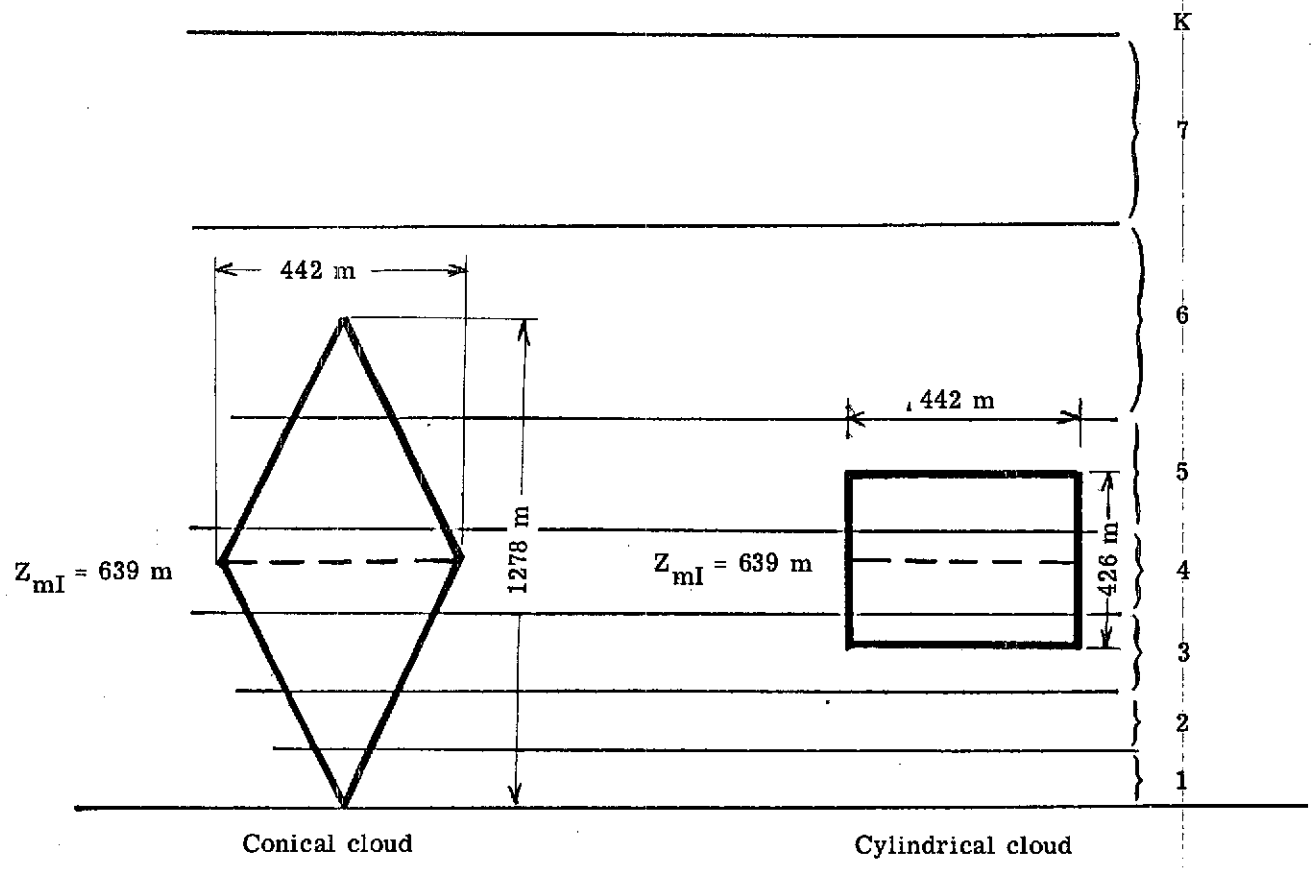

Figure 6.- Stabilized cloud geometries with equal volumes and equal crosswind and alongwind dimensions at cloud centroid for a low-level sea-breeze meteorological regime at Kennedy Space Center.

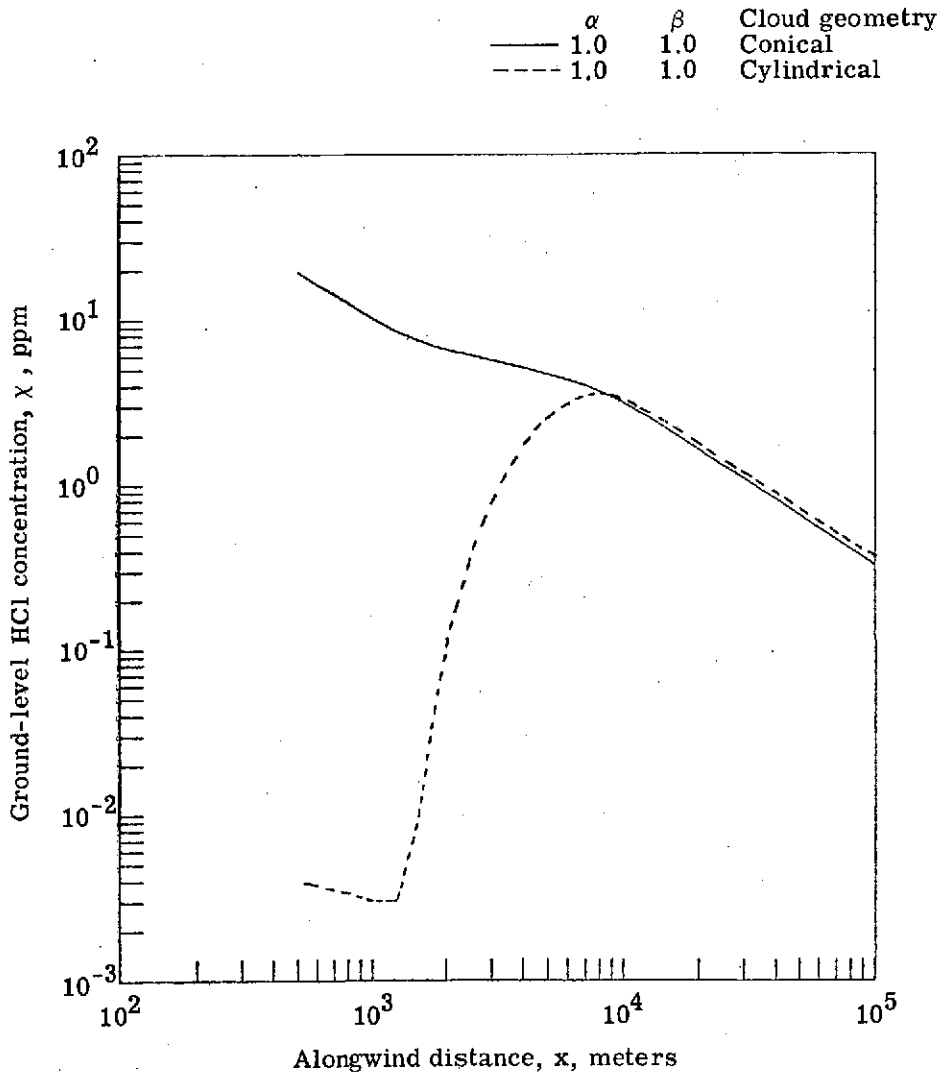

Figure 7.- Peak ground-level HCl concentration as a function of alongwind distance from cloud stabilization for a low-level sea-breeze meteorological regime.

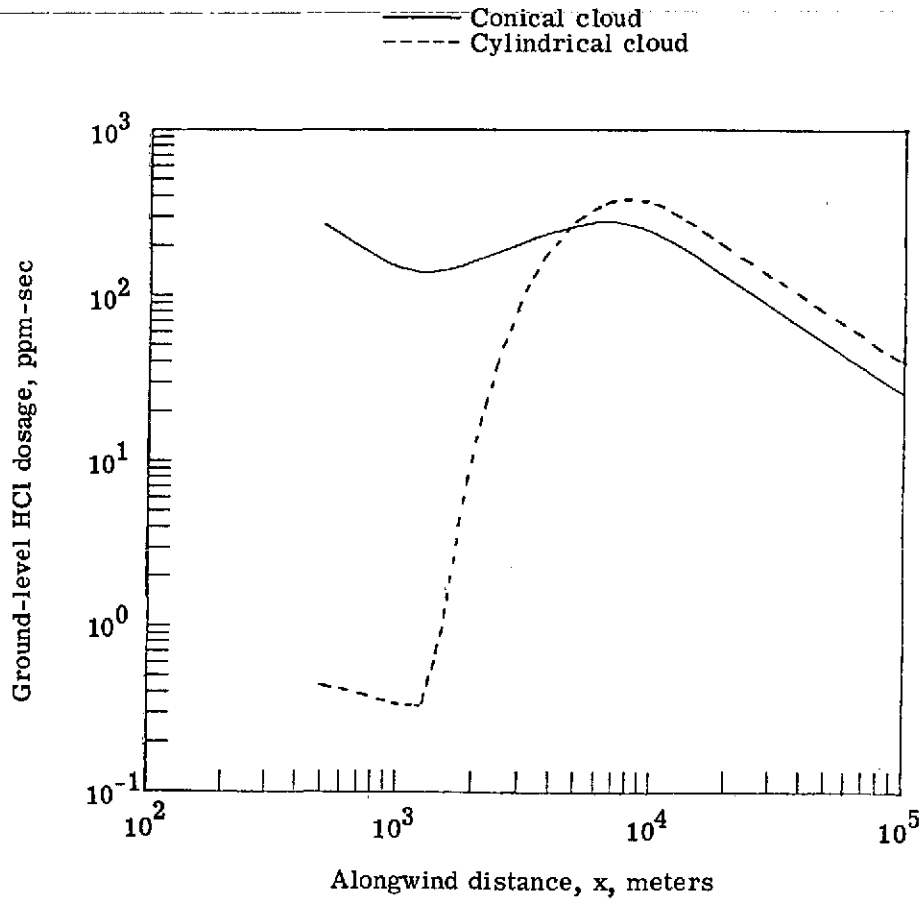

Figure 8.- Peak ground-level HCl dosage as a function of alongwind distance from cloud stabilization for a low-level sea-breeze meteorological regime.

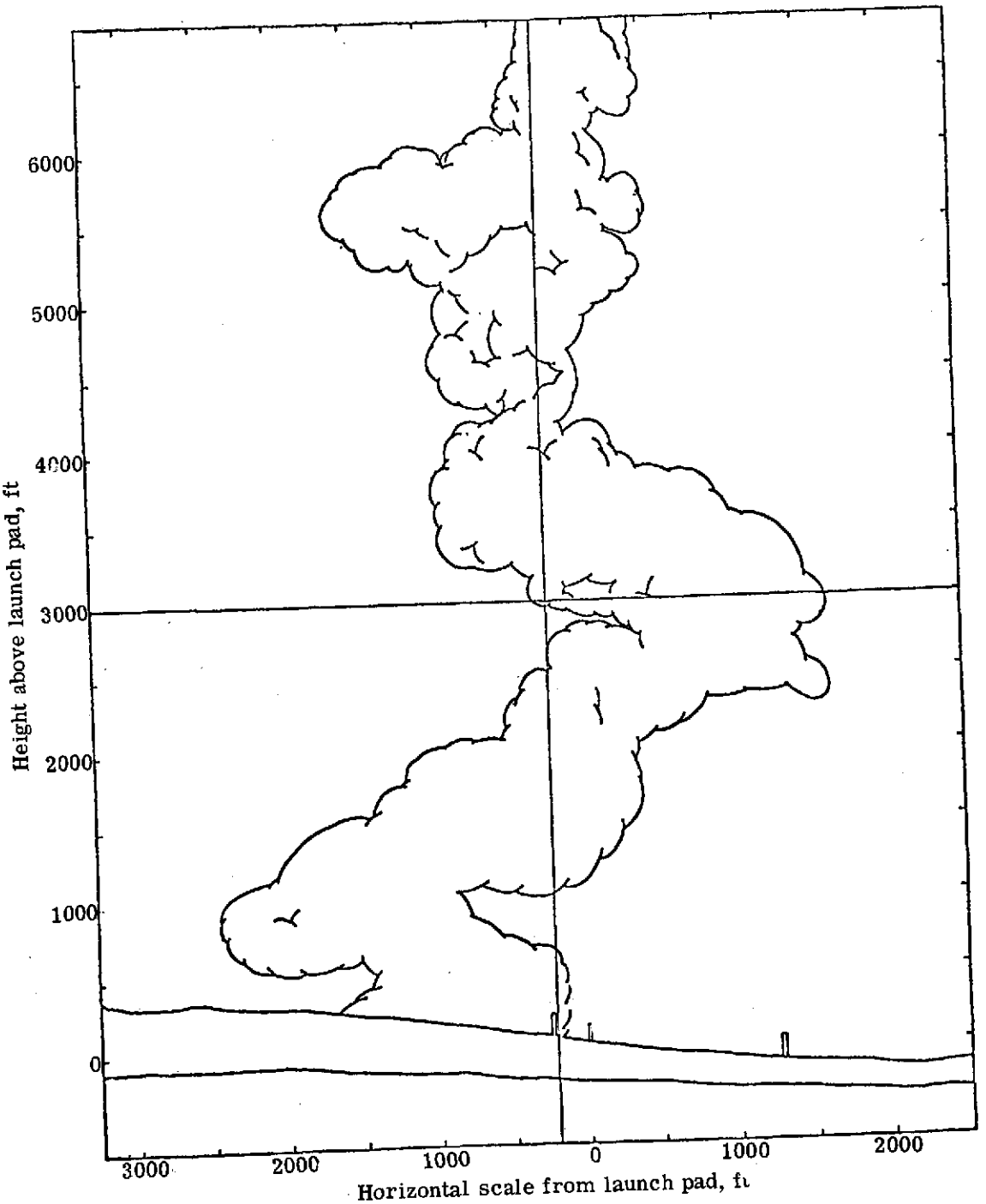

(a) Exhaust cloud at t + 185 seconds from camera site 020P50.

Figure 9.- Titan III exhaust-cloud sketches from Vandenberg Air Force Base camera sites.

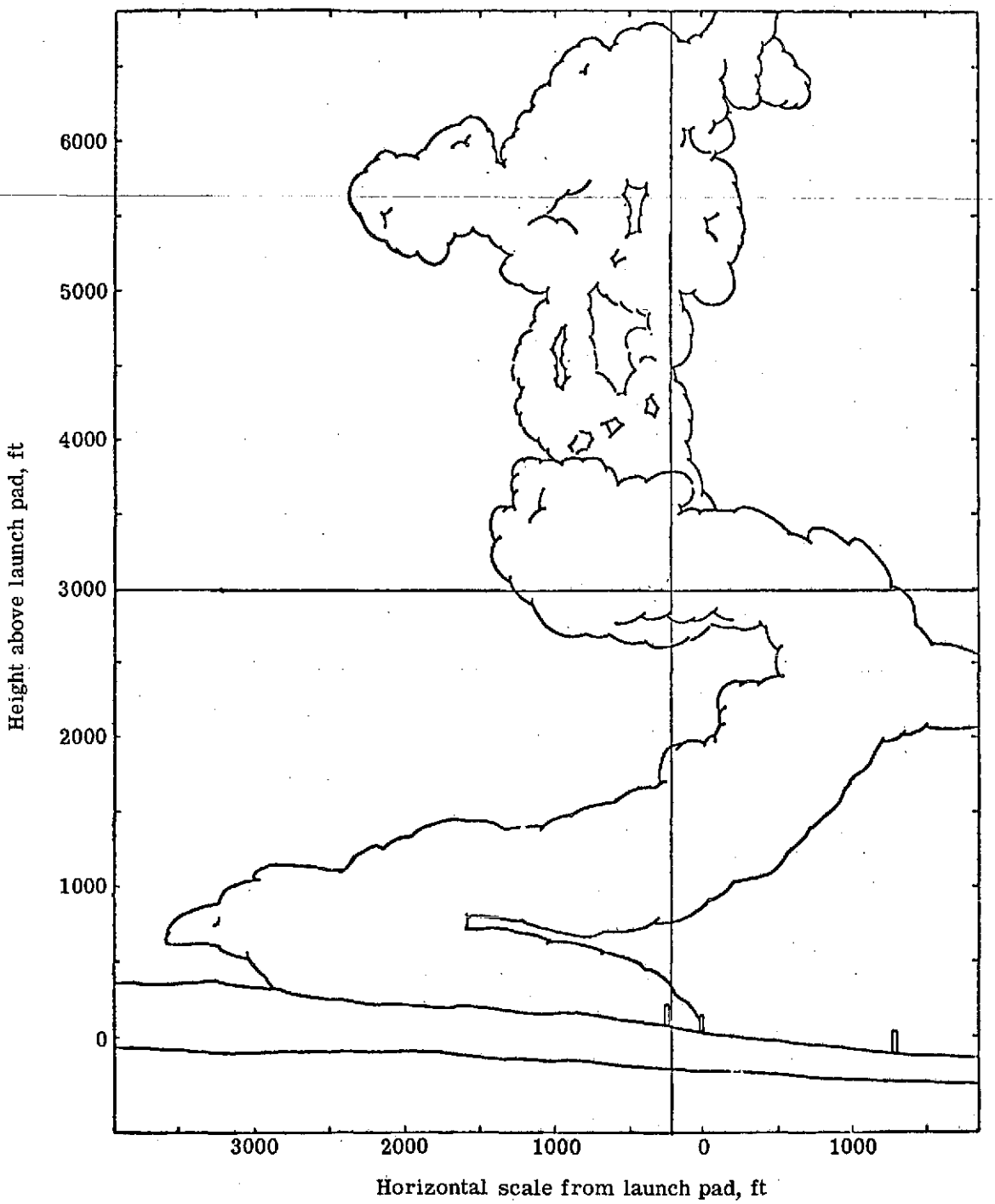

(b) Exhaust cloud at t + 305 seconds from camera site 020P50.

Figure 9.- Continued.

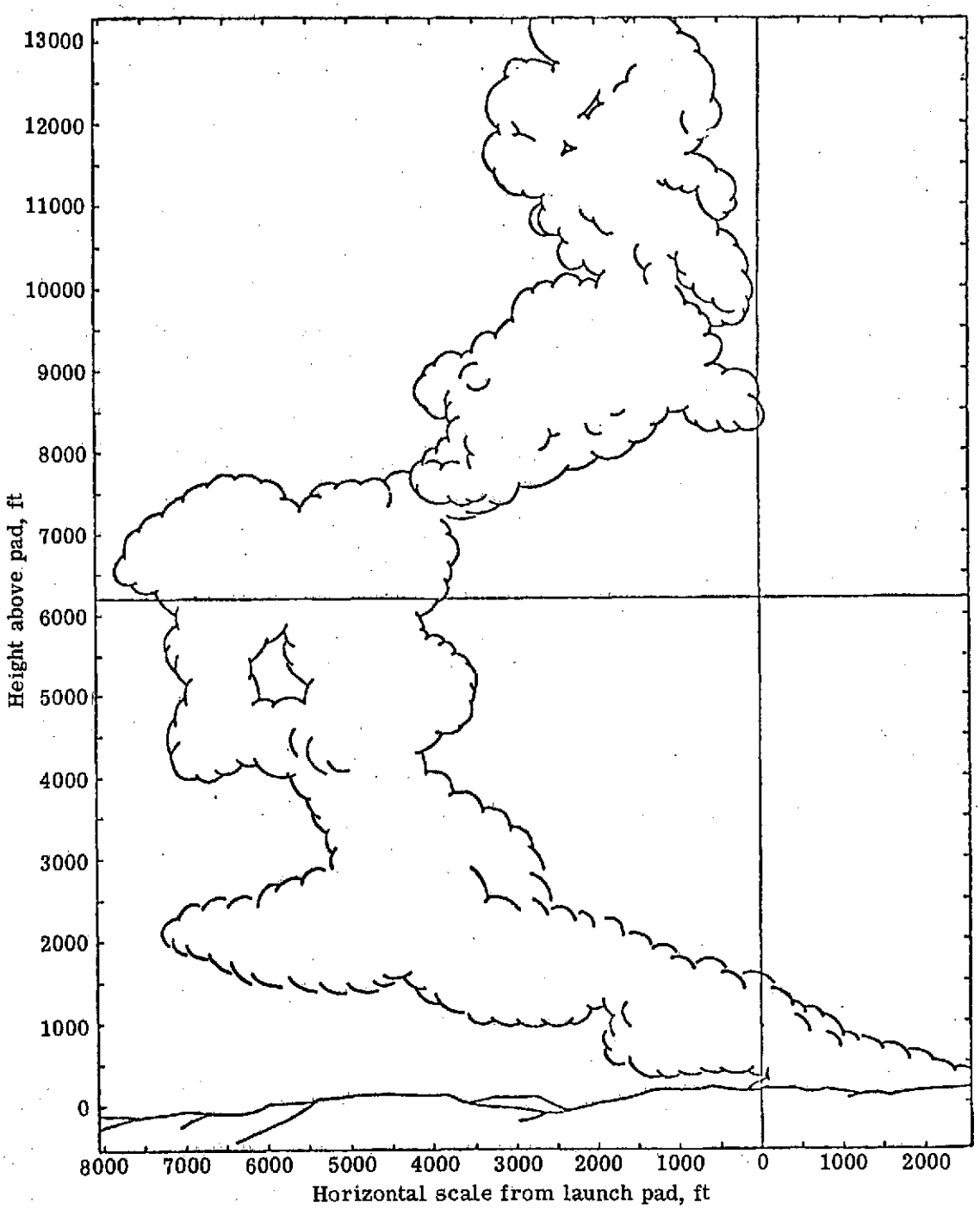

(c) Exhaust cloud at t + 305 seconds from camera site 020P91.

Figure 9.- Continued.

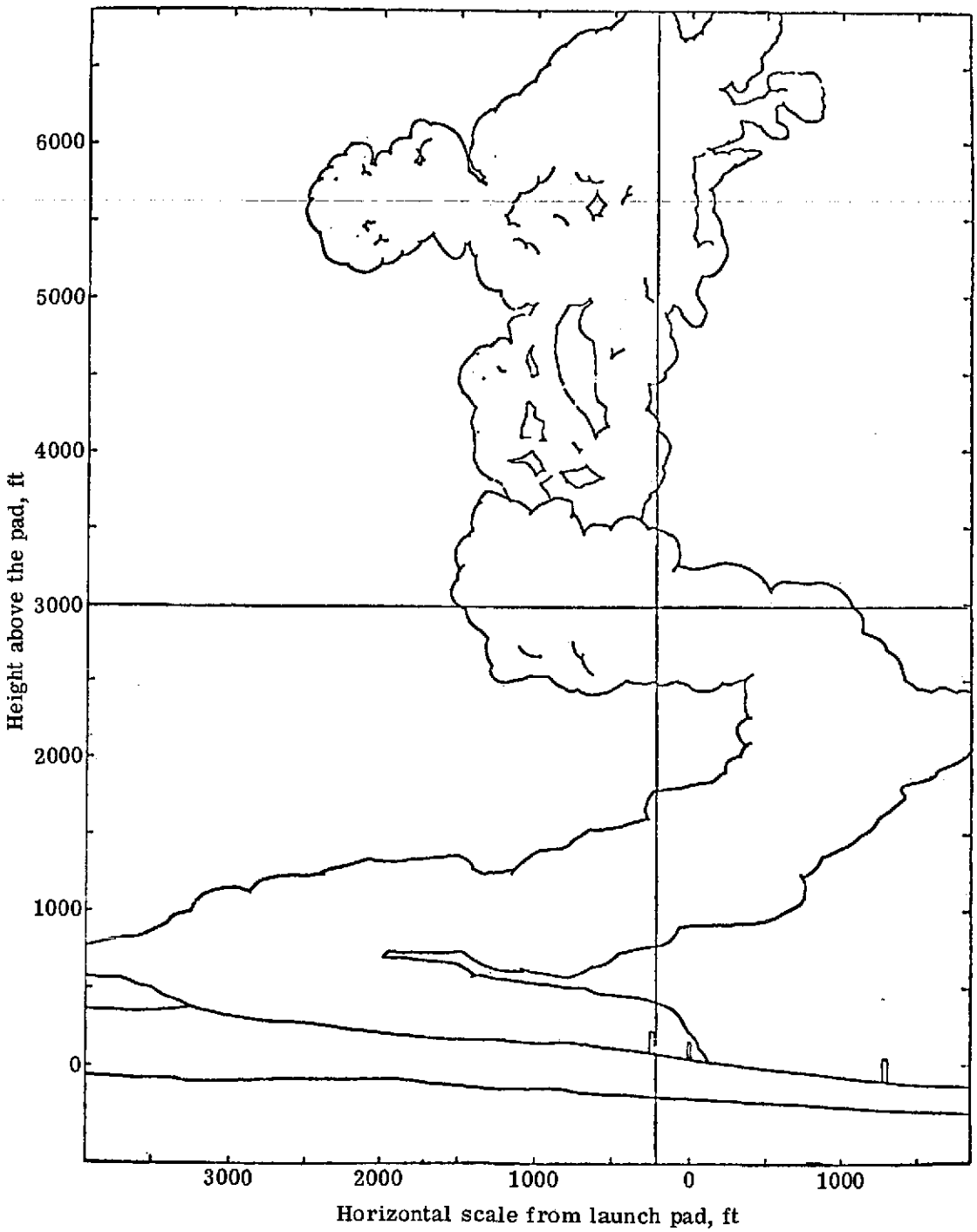

(d) Exhaust cloud at t + 365 seconds from camera site 020P50.

Figure 9.- Concluded.

(a) Early time.

Figure 10.- Titan III ground-cloud photographs from Kennedy Space Center.

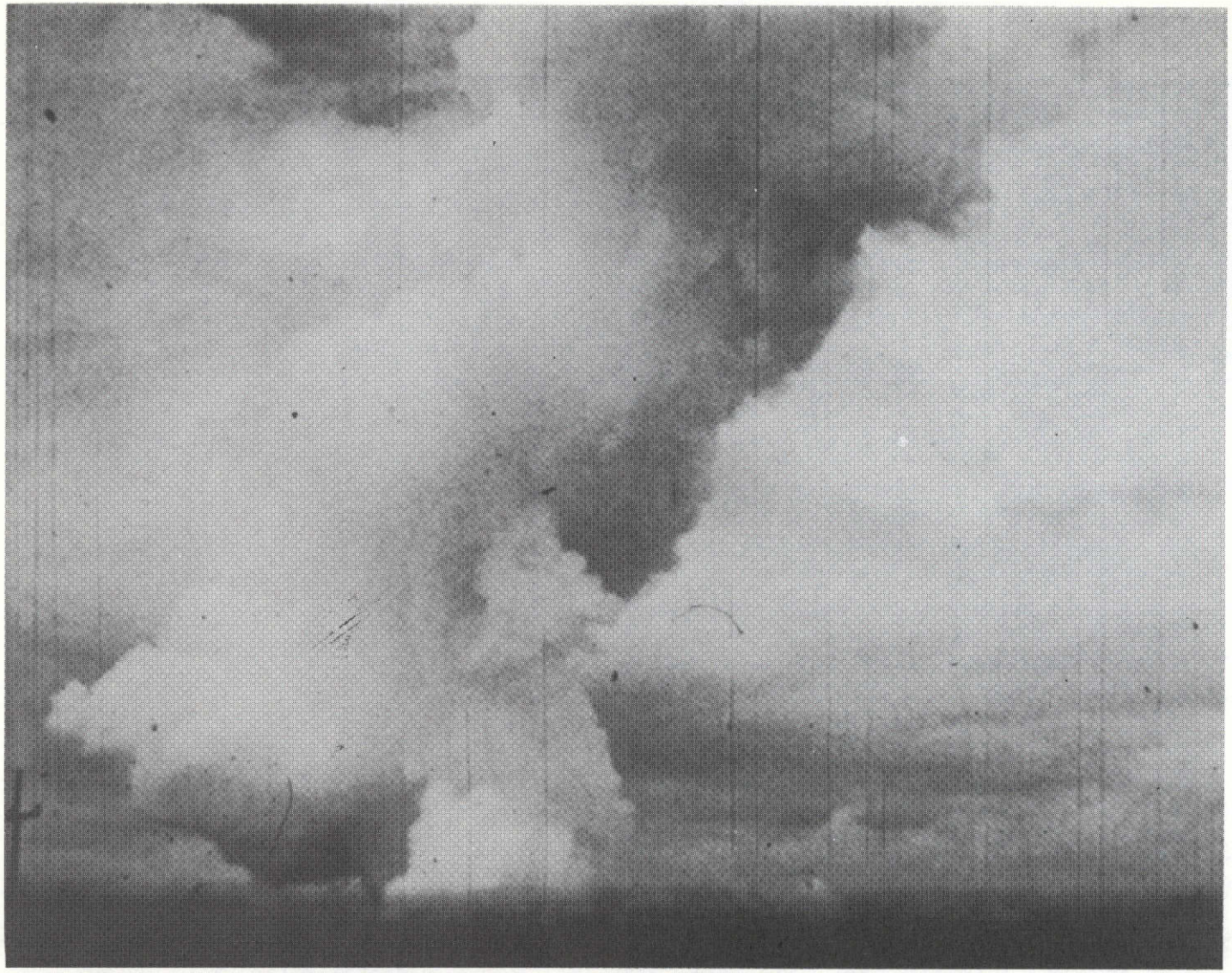

(b) Intermediate time.

Figure 10.- Continued.

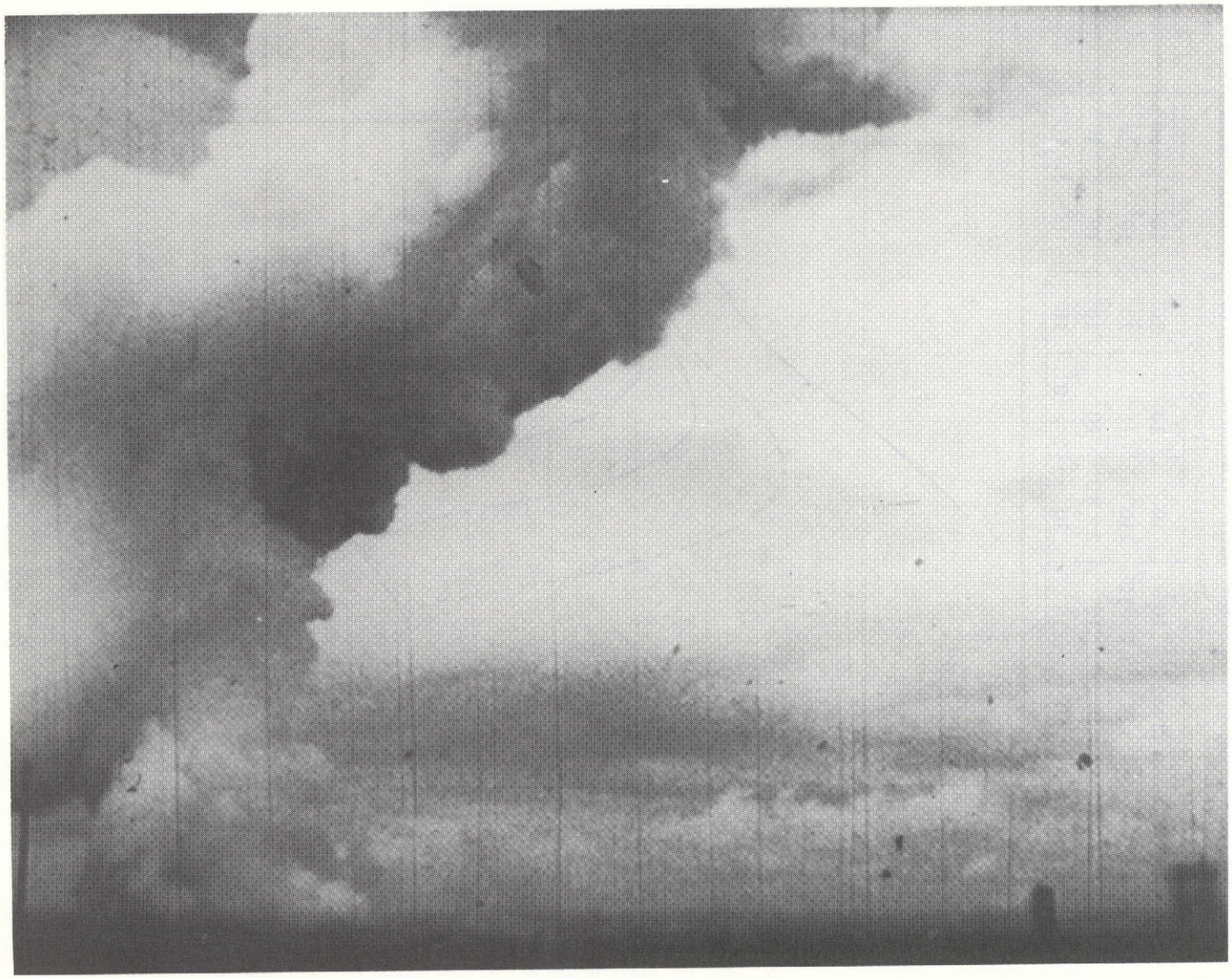

(c) Late time.

Figure 10.- Concluded.

VERTICAL SOURCE-TERM VARIATIONS, Q_K, ppm-m^2

Z_{TK}, m	150	300	500	700	1000	1500	2000
	Layer source strength, ppm-m^2						
———	2×10^7	10^3	10^3	10^3	10^3	10^3	10^3
– – – –	10^3	2×10^7	10^3	10^3	10^3	10^3	10^3
— – —	10^3	10^3	2×10^7	10^3	10^3	10^3	10^3
— – – —	10^3	10^3	10^3	2×10^7	10^3	10^3	10^3

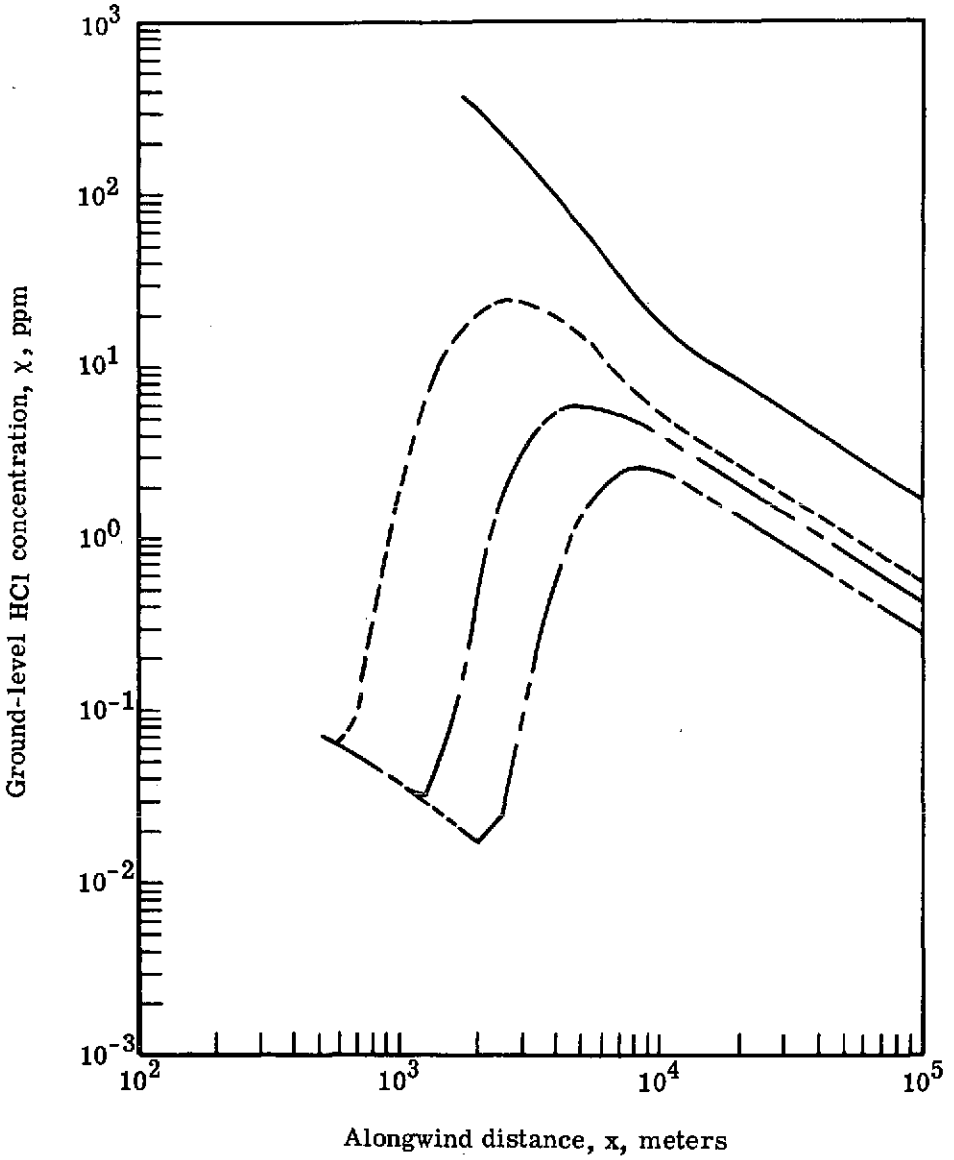

(a) For a conical cloud.

Figure 11.- Ground-level HCl concentrations with variations of the source-term distributions for a low-level sea-breeze meteorological regime.

VERTICAL SOURCE-TERM VARIATIONS, Q_K, ppm-m^2

Z_{TK}, m	150	300	500	700	6000	1500	2000
	Layer source strength, ppm-m^2						
———	2×10^7	10^3	10^3	10^3	10^3	10^3	10^3
- - - - - -	10^3	2×10^7	10^3	10^3	10^3	10^3	10^3
— - - —	10^3	10^3	2×10^7	10^3	10^3	10^3	10^3
— - - —	10^3	10^3	10^3	2×10^7	10^3	10^3	10^3

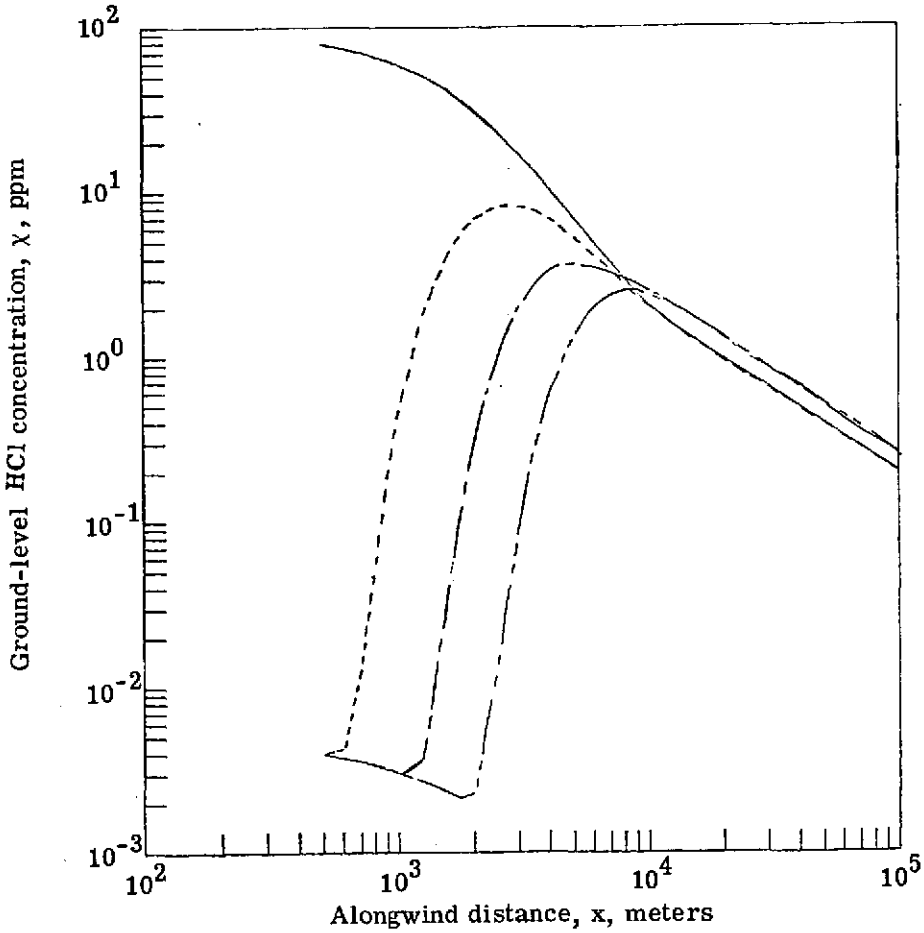

(b) For a cylindrical cloud.

Figure 11.- Concluded.

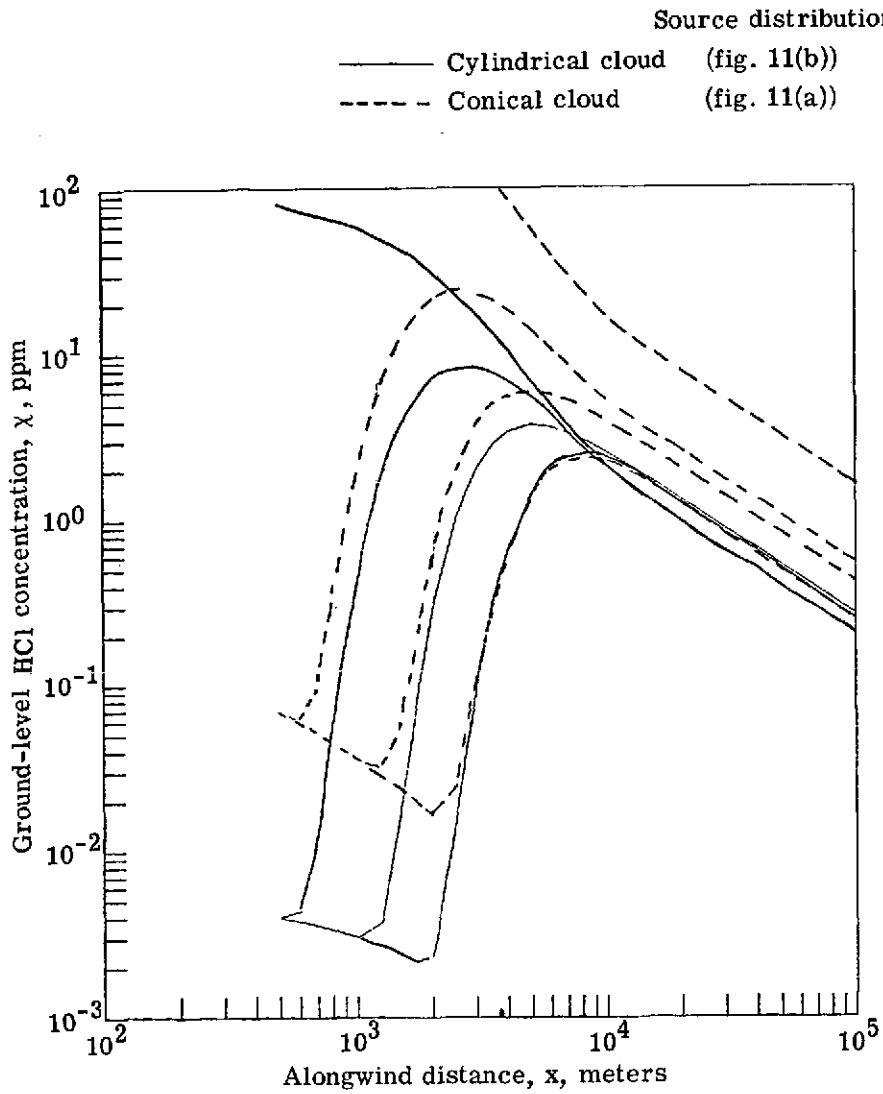

Figure 12.- Ground-level HCl concentrations for conical and cylindrical clouds with source-term variations for a low-level sea-breeze meteorological regime.

	Vertical mass distribution	Cloud geometry	α	β
———	Uniform	Cylindrical	1.0	1.0
– – – –	Gaussian	Conical	1.0	1.0
— – —	Uniform	Cylindrical	.5	1.0
— – – —	Gaussian	Conical	.5	1.0

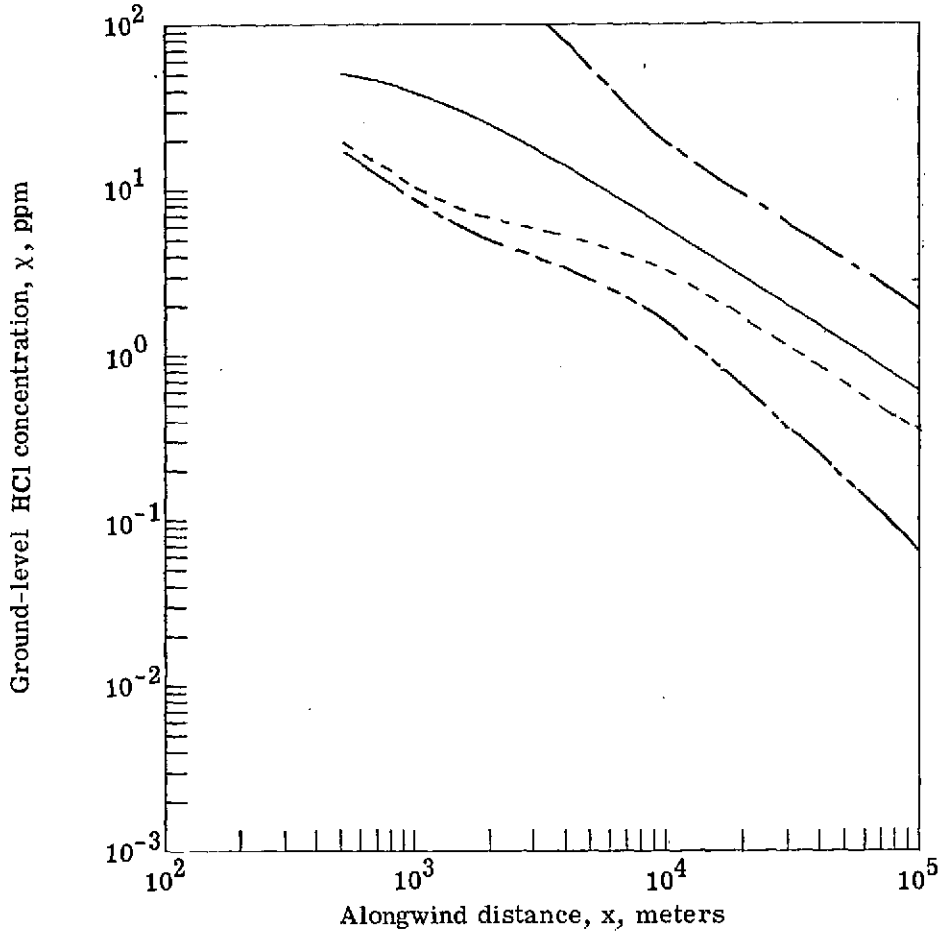

Figure 13.- Ground-level HCl concentrations for conical and cylindrical clouds with uniform and Gaussian mass loading in the clouds for a low-level sea-breeze meteorological regime. (Total HCl mass loading is conserved between both cloud geometries.)

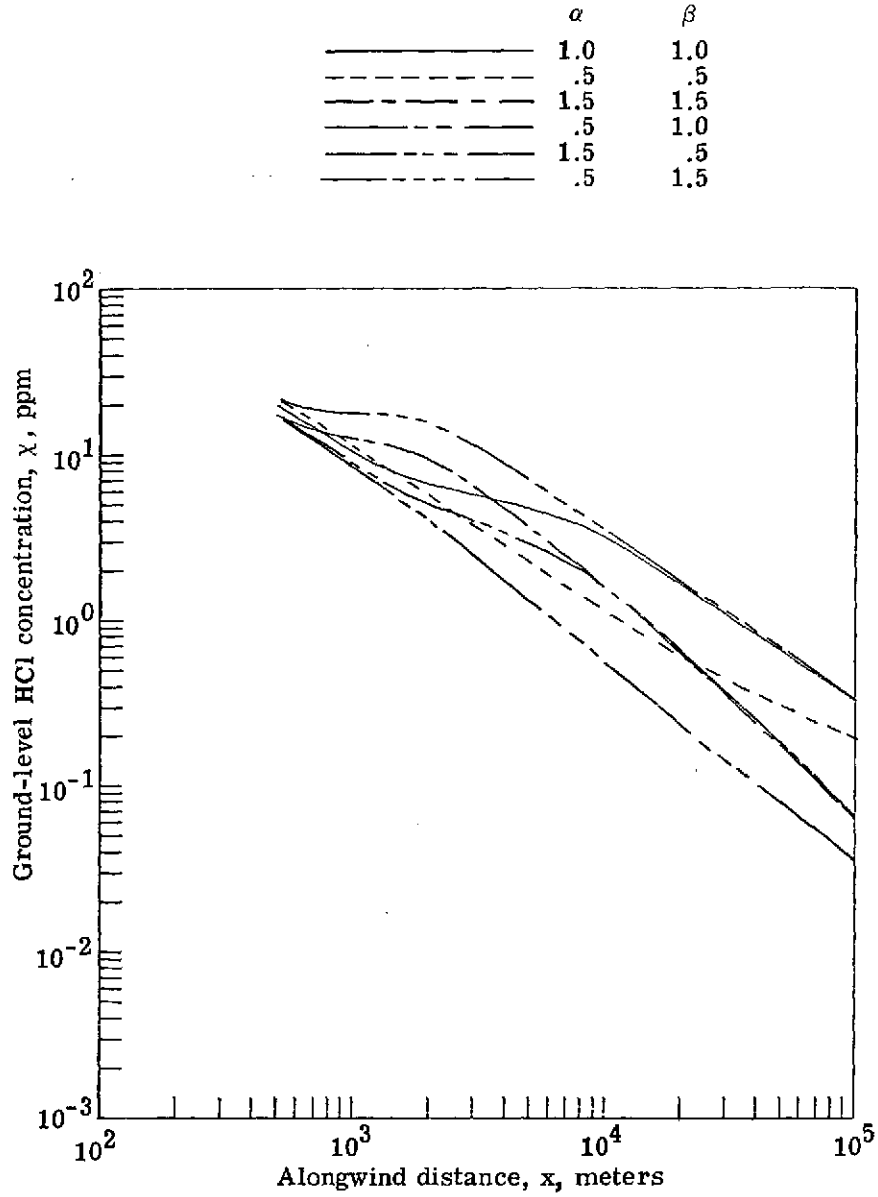

Figure 14.- Ground-level HCl concentrations for conical clouds with variations of the lateral and vertical diffusion exponents for a low-level sea-breeze meteorological regime.

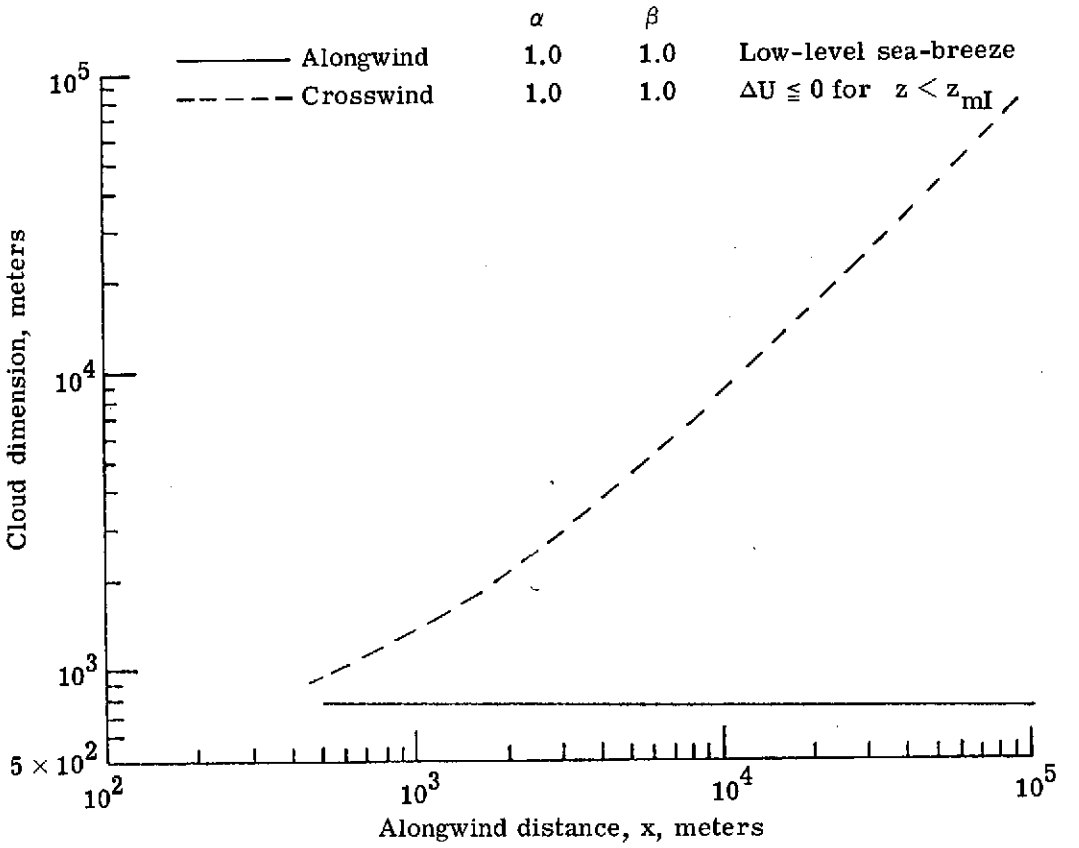

Figure 15.- Conical ground-cloud growth with alongwind distance for a low-level sea-breeze meteorological regime at Kennedy Space Center.

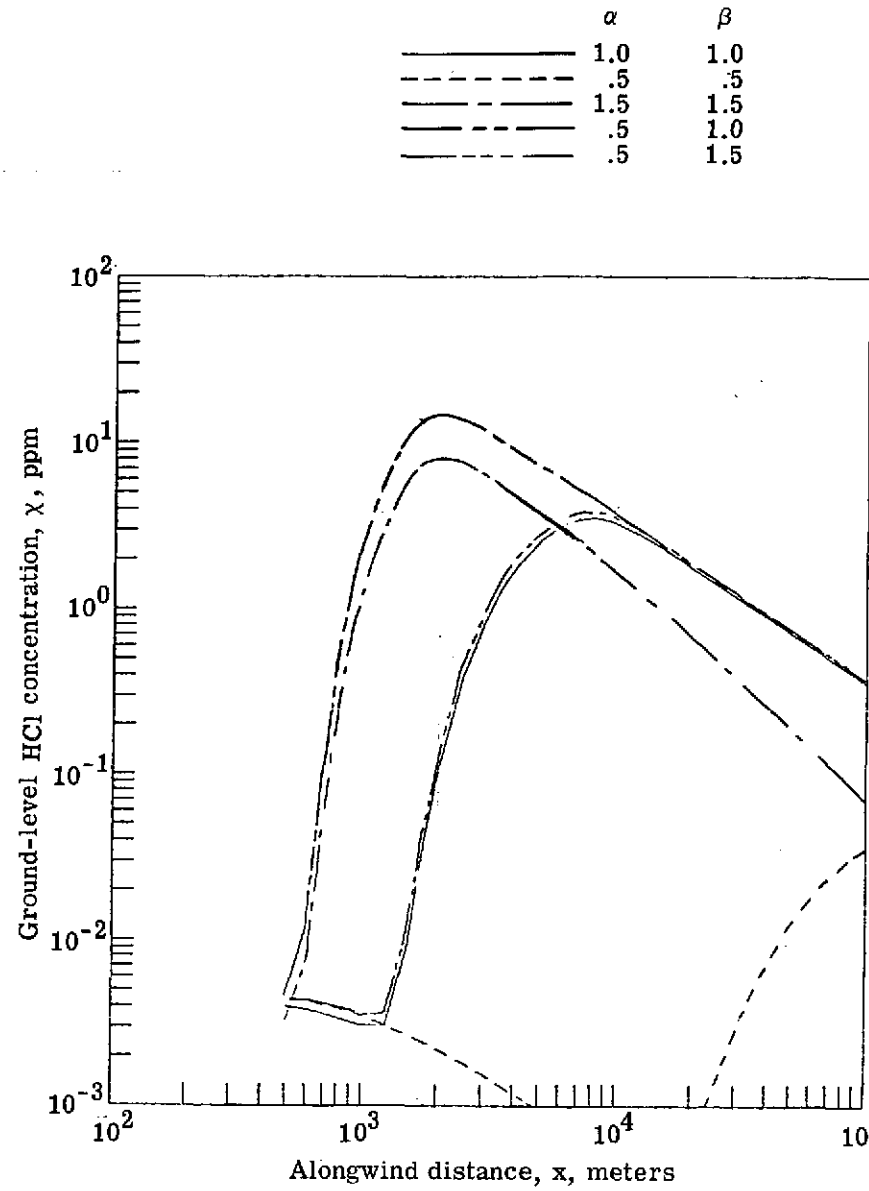

Figure 16.- Ground-level HCl concentrations for cylindrical clouds with variations of the lateral and vertical diffusion exponents for a low-level sea-breeze meteorological regime.

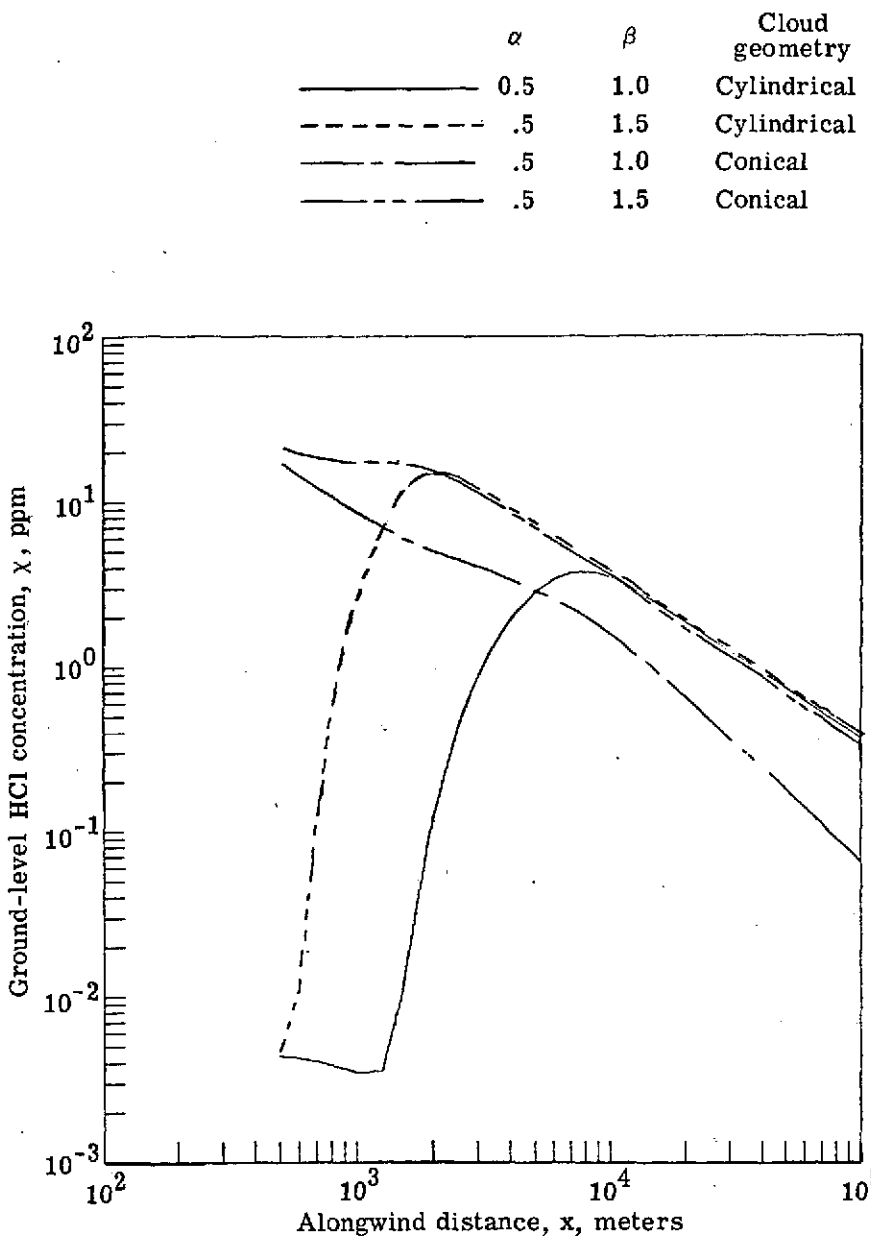

Figure 17.- Comparison of ground-level HCl concentrations for conical and cylindrical clouds with two sets of lateral and vertical diffusion exponents for a low-level sea-breeze meteorological regime.

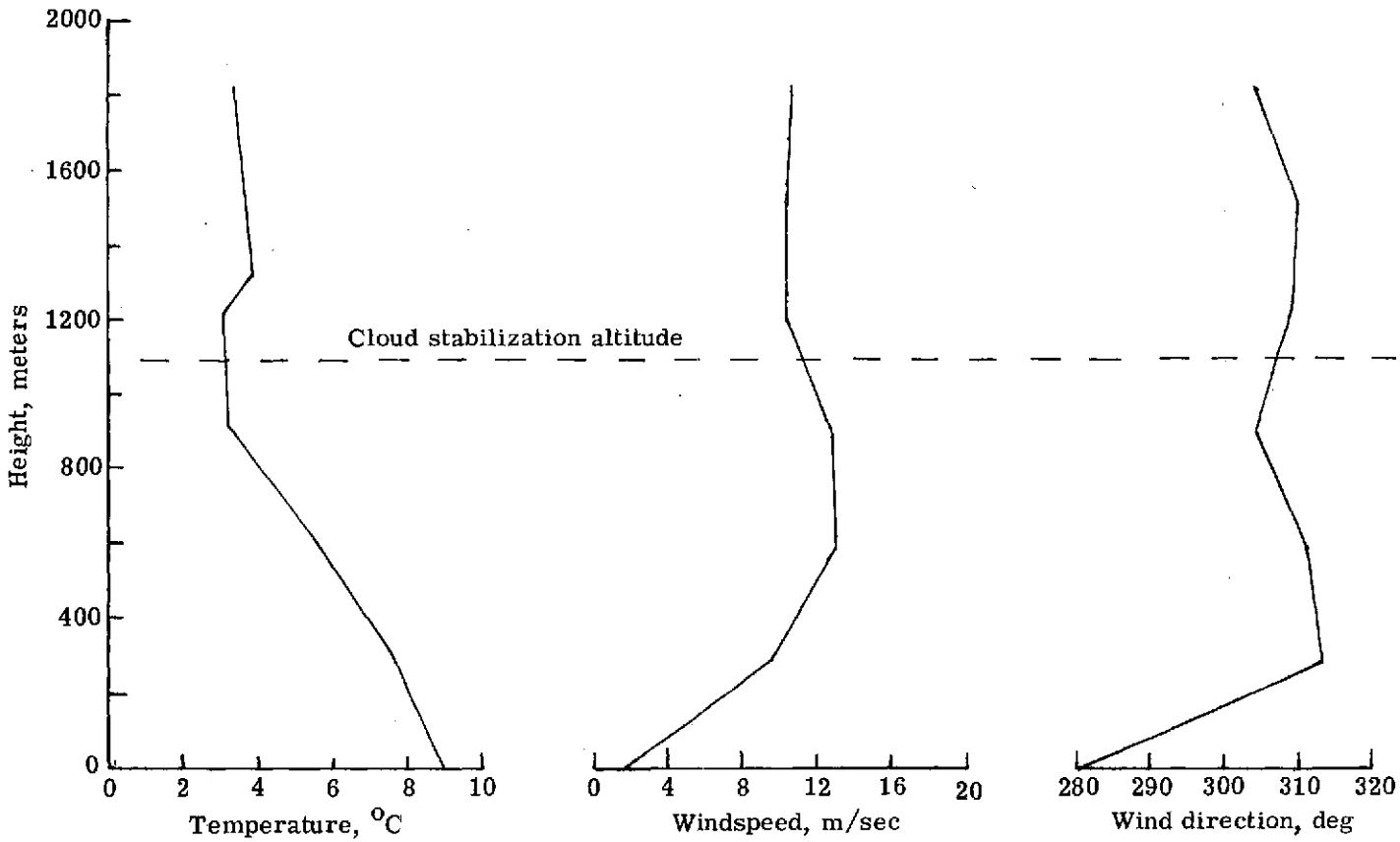

Figure 18.- Measured vertical profiles of temperature, windspeed, and wind direction at launch on February 11, 1974 at Kennedy Space Center.

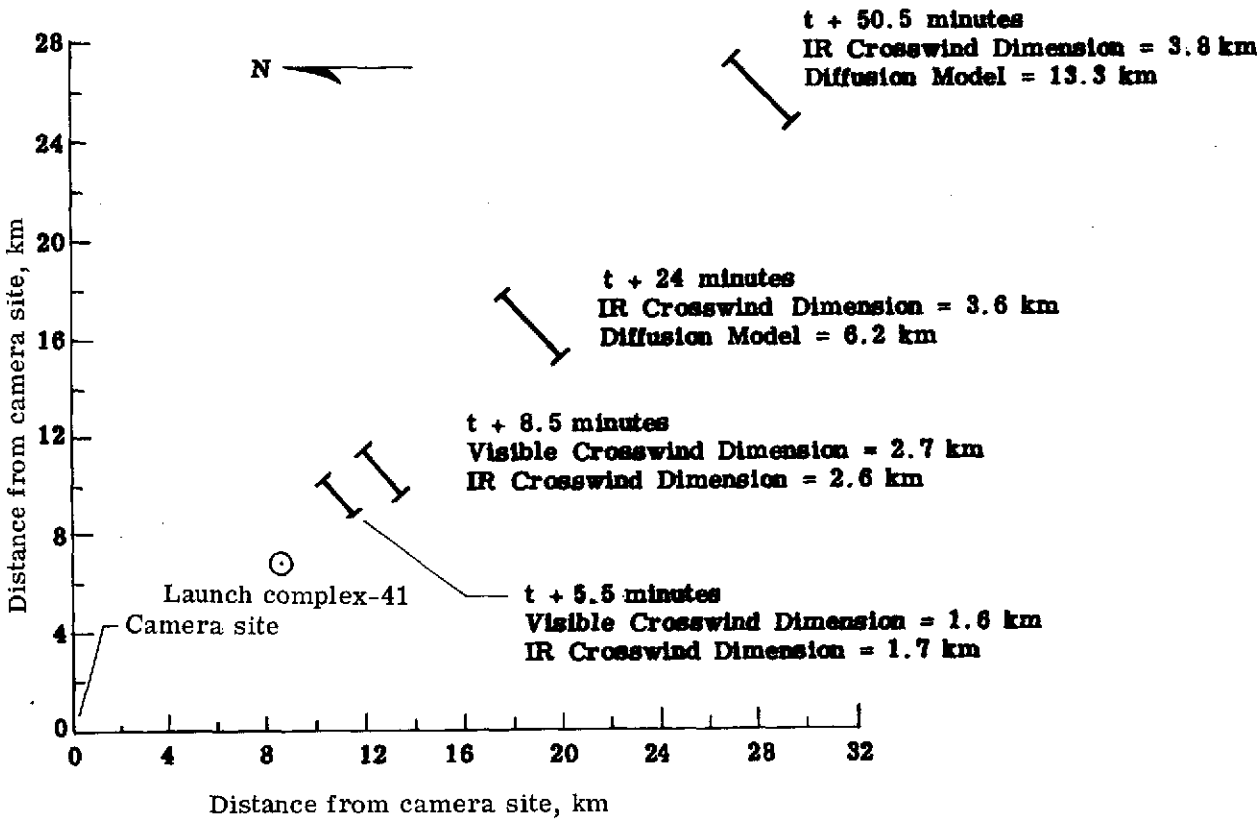

Figure 19.- Measured and calculated cloud crosswind dimensions following launch on February 11, 1974 at Kennedy Space Center.

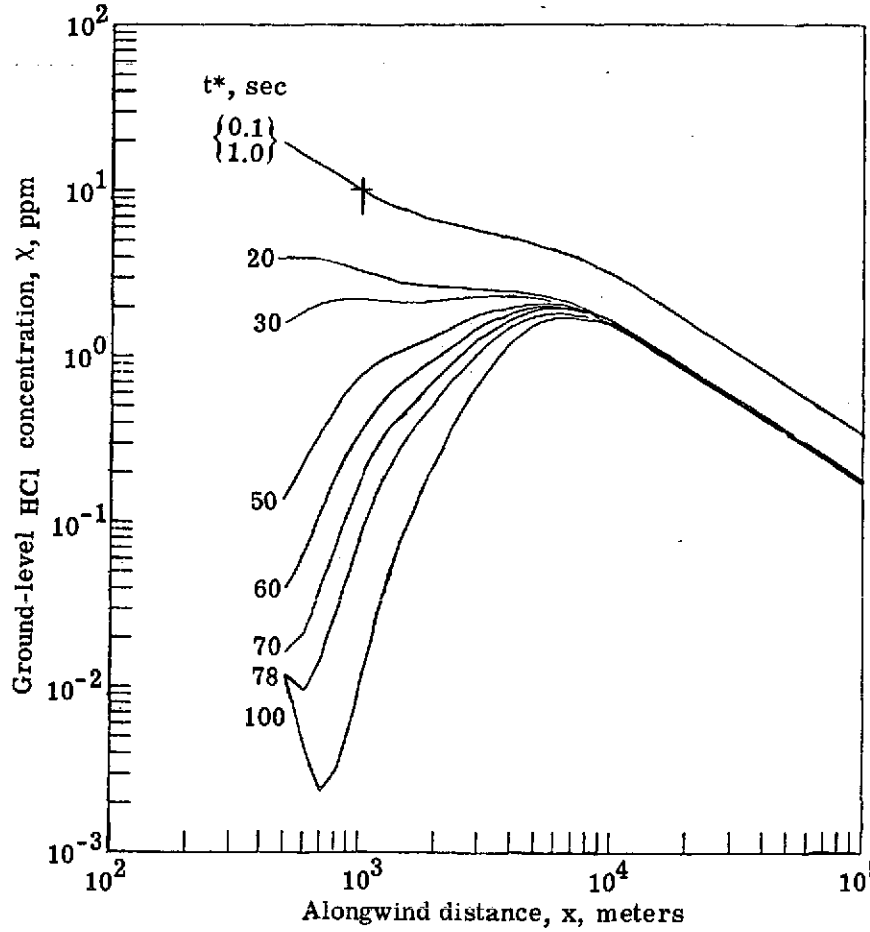

Figure 20.- Ground-level HCl concentration variations with distance and assumed time of layer transition for conical clouds with a low-level sea-breeze meteorological regime. α = 1.0, β = 1.0.

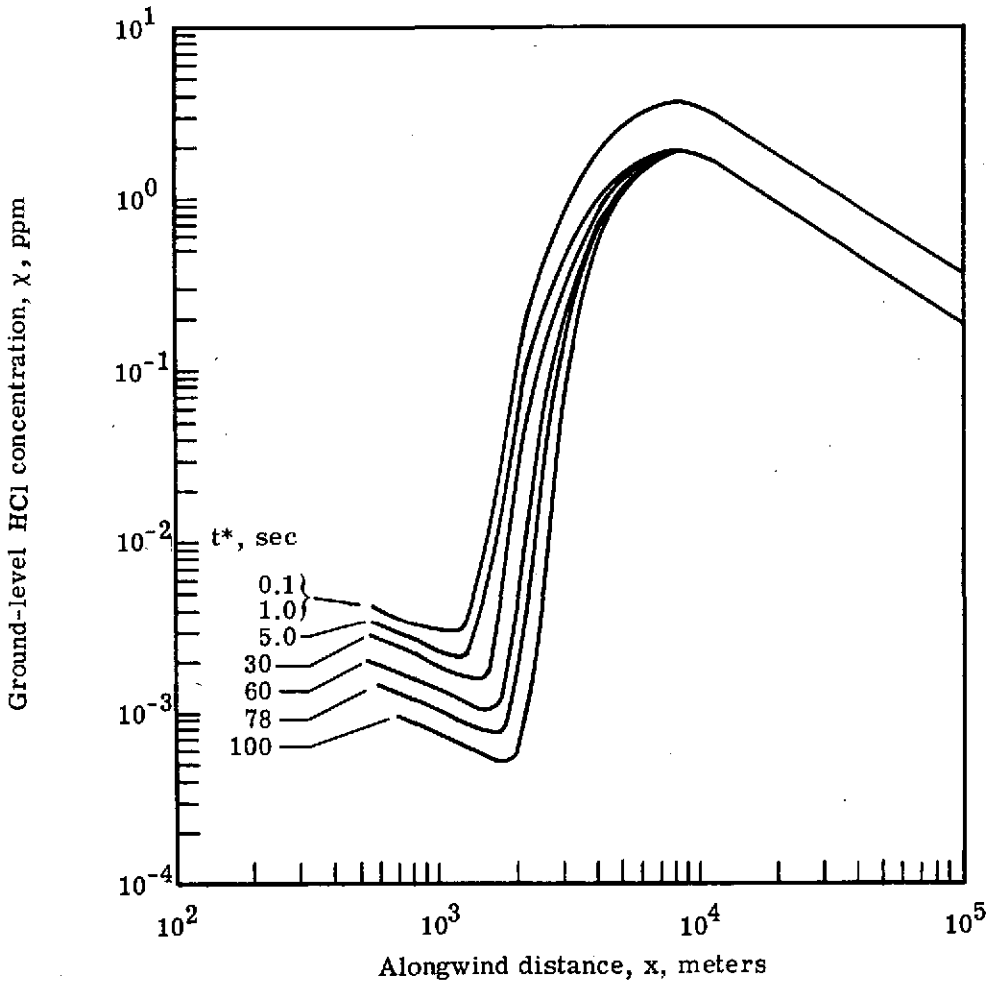

Figure 21.- Ground-level HCl concentration variations with distance and assumed time of layer transition for cylindrical clouds with a low-level sea-breeze meteorological regime. α = 1.0, β = 1.0.

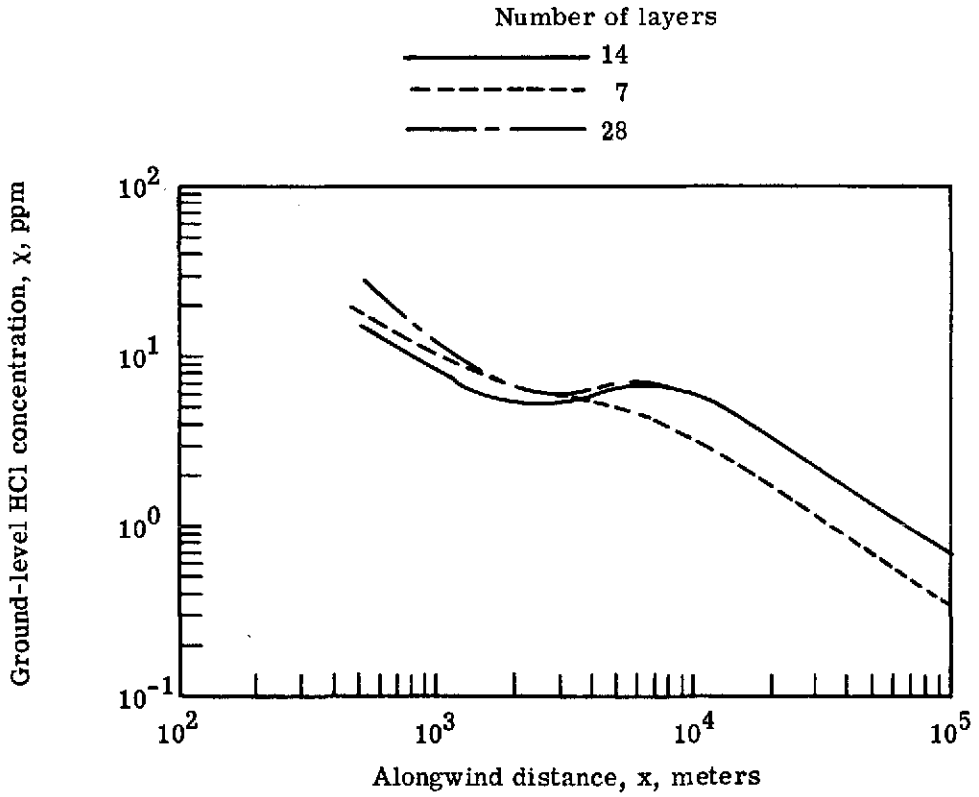

Figure 22.- Ground-level HCl concentration variations with distance and assumed layer division for conical clouds with a low-level sea-breeze meteorological regime. α = 1.0, β = 1.0.

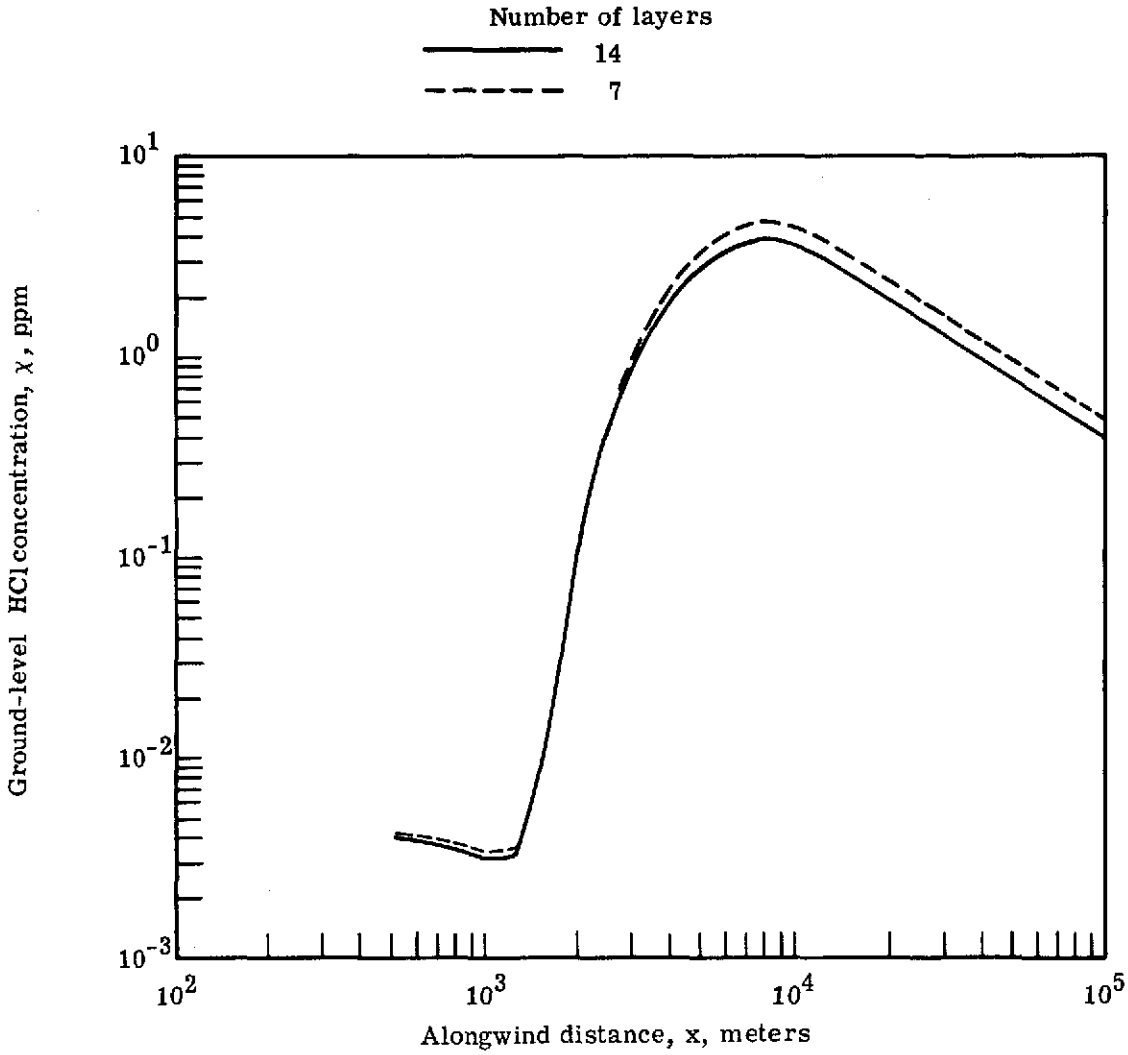

Figure 23.- Ground-level HCl concentration variations with distance and assumed layer division for cylindrical clouds with a low-level sea-breeze meteorological regime. α = 1.0, β = 1.0.

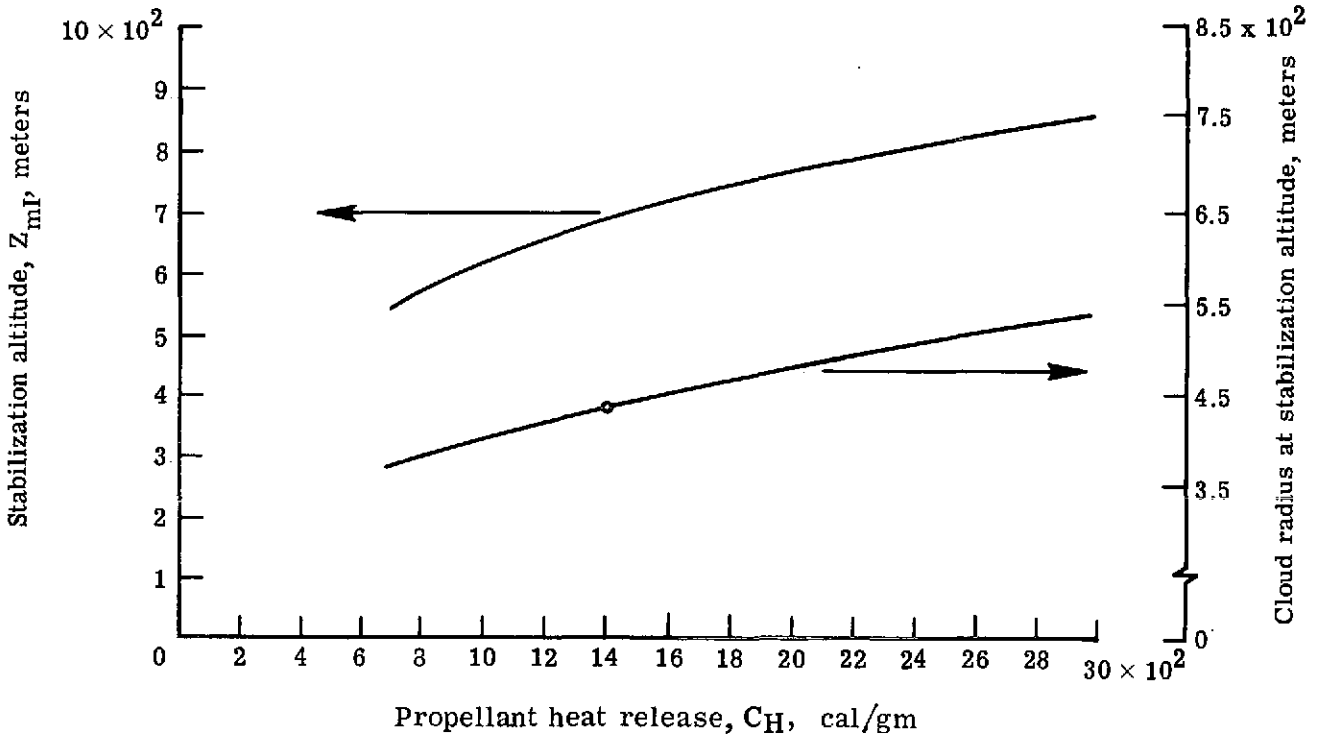

Figure 24.- Conical-cloud stabilization height and growth as functions of effective heat release for a Titan III-E rocket in a low-level sea-breeze meteorological regime at Kennedy Space Center.

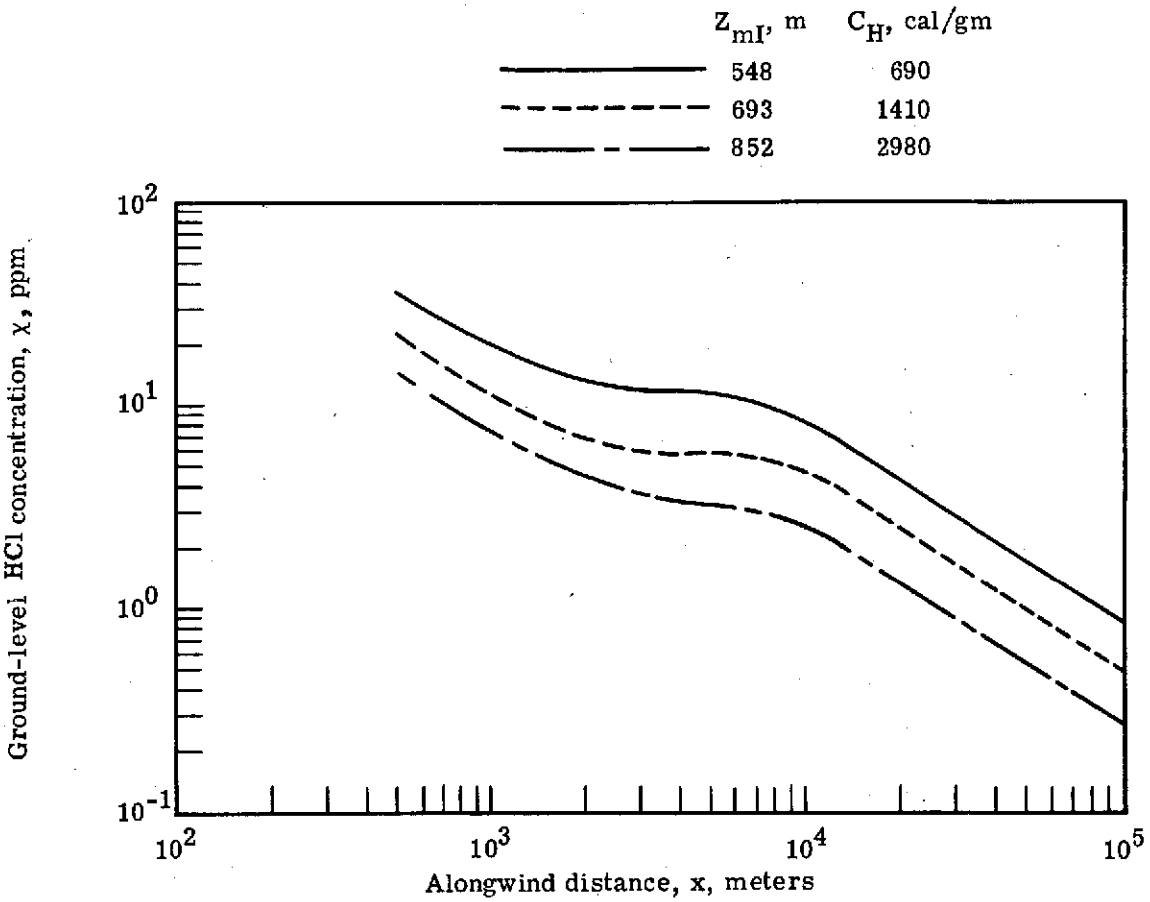

Figure 25.- Ground-level HCl concentration as a function of distance and effective engine-heat release for a Titan III-E rocket in a low-level sea-breeze meteorological regime at Kennedy Space Center. $\alpha = 1.0$, $\beta = 1.0$.

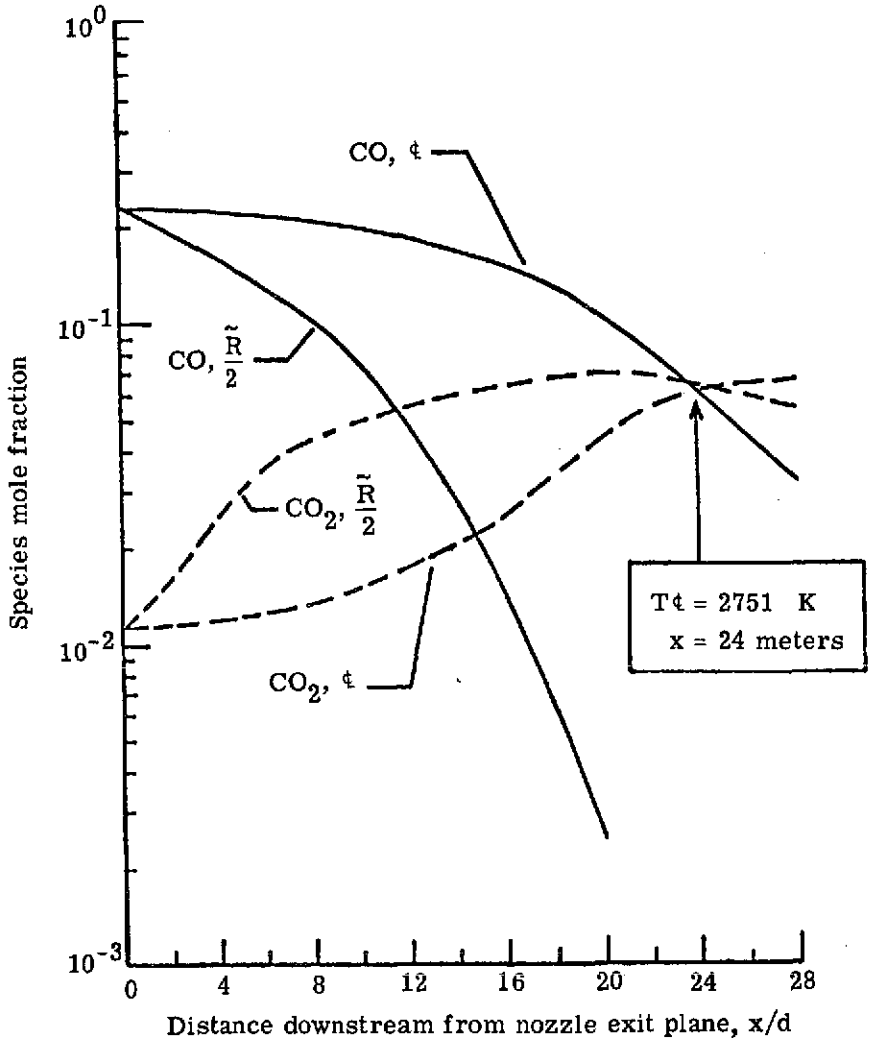

Figure 26.- CO and CO_2 mole fractions as functions of distance from the rocket-nozzle exit plane for a full-scale Castor II solid motor. d, exit plane diameter; $\tilde{R}/2$, plume half-radius.

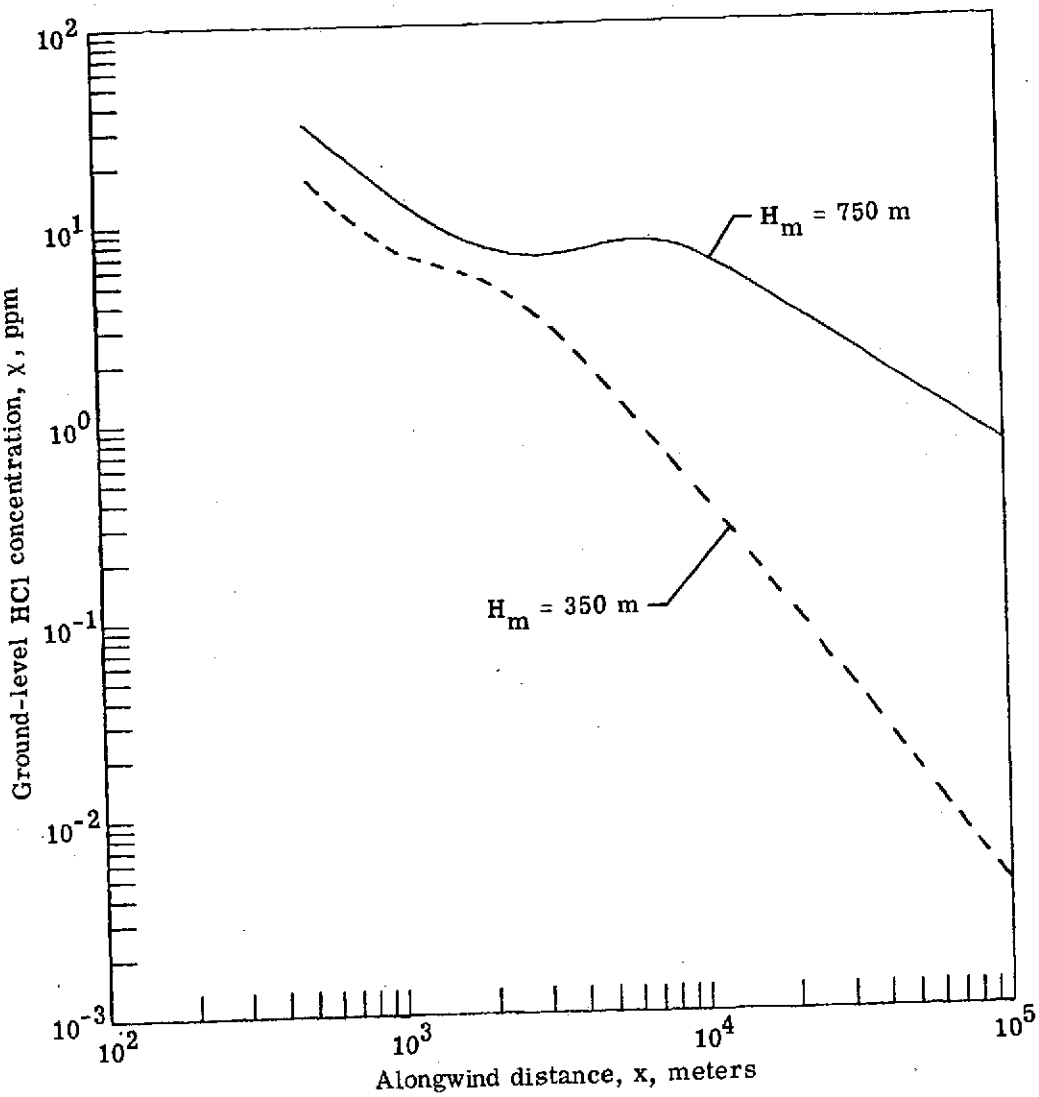

Figure 27.- Ground-level HCl concentration variations as functions of distance and assumed mixing-layer depth for a low-level sea-breeze meteorological regime. (Conical clouds with Gaussian mass distribution.) $\alpha = 0.5$, $\beta = 1.0$.

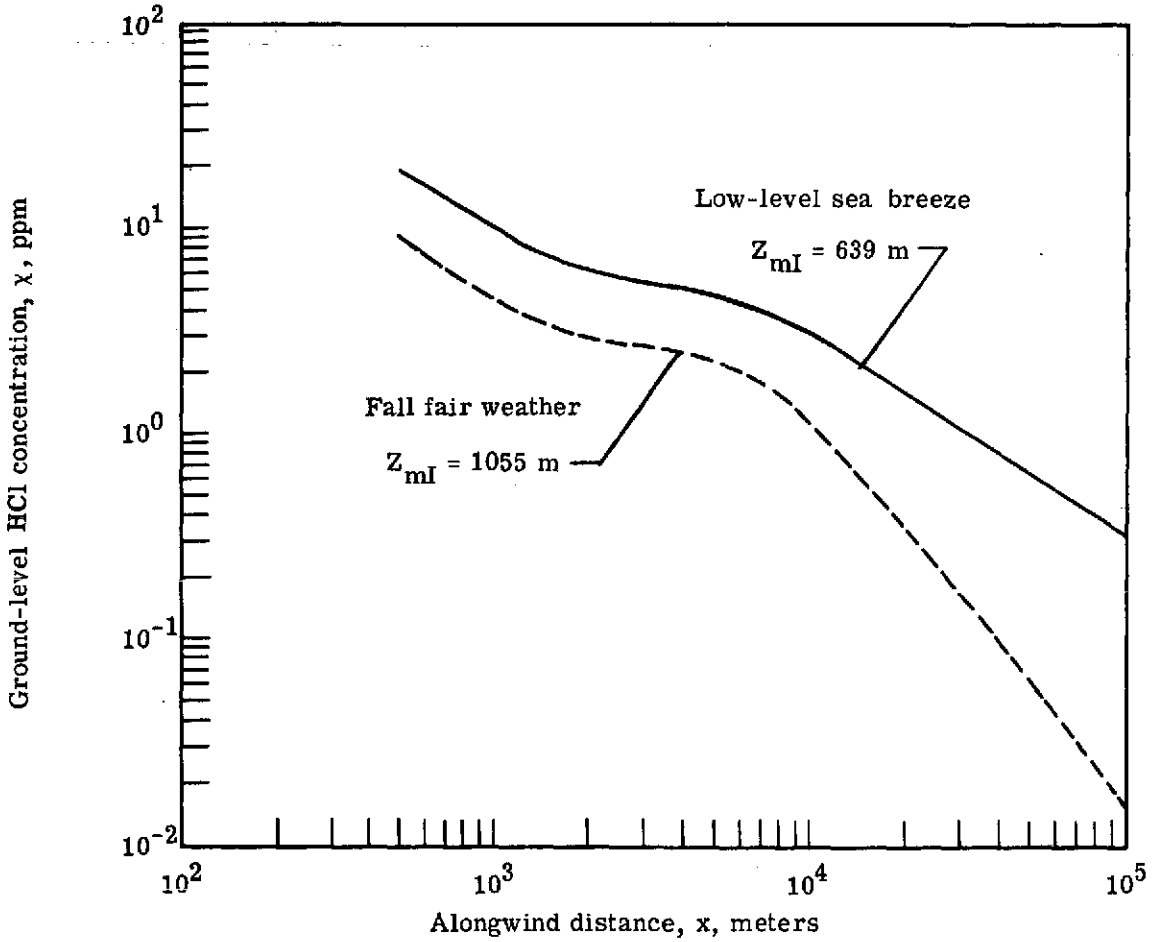

Figure 28.- Ground-level HCl concentration variation with distance for two characteristic meteorological regimes at Kennedy Space Center. (Conical clouds.)

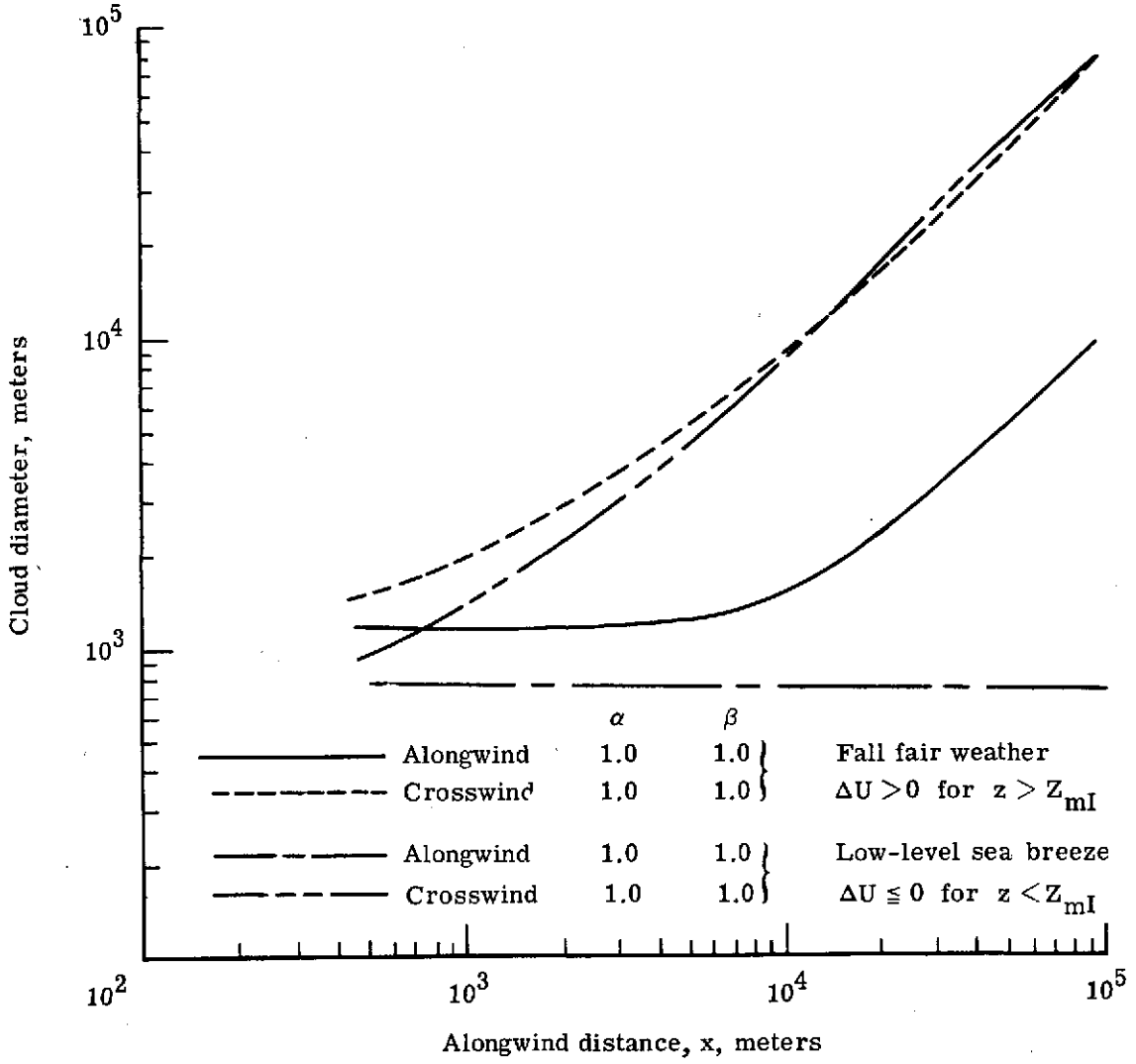

Figure 29.- Conical ground-cloud growth for fall fair weather and low-level sea-breeze meteorological regimes at Kennedy Space Center.